nature medicine

Article

https://doi.org/10.1038/s41591-024-03209-x

Brain clocks capture diversity and disparities in aging and dementia across geographically diverse populations

Received: 22 March 2024

Accepted: 22 July 2024

Published online: 26 August 2024

Check for updates

A list of authors and their affiliations appears at the end of the paper

Brain clocks, which quantify discrepancies between brain age and chronological age, hold promise for understanding brain health and disease. However, the impact of diversity (including geographical, socioeconomic, sociodemographic, sex and neurodegeneration) on the brain-age gap is unknown. We analyzed datasets from 5,306 participants across 15 countries (7 Latin American and Caribbean countries (LAC) and 8 non-LAC countries). Based on higher-order interactions, we developed a brain-age gap deep learning architecture for functional magnetic resonance imaging (2,953) and electroencephalography (2,353). The datasets comprised healthy controls and individuals with mild cognitive impairment, Alzheimer disease and behavioral variant frontotemporal dementia. LAC models evidenced older brain ages (functional magnetic resonance imaging: mean directional error = 5.60, root mean square error (r.m.s.e.) = 11.91; electroencephalography: mean directional error = 5.34, r.m.s.e. = 9.82) associated with frontoposterior networks compared with non-LAC models. Structural socioeconomic inequality, pollution and health disparities were influential predictors of increased brain-age gaps, especially in LAC (R^2 = 0.37, F^2 = 0.59, r.m.s.e. = 6.9). An ascending brain-age gap from healthy controls to mild cognitive impairment to Alzheimer disease was found. In LAC, we observed larger brain-age gaps in females in control and Alzheimer disease groups compared with the respective males. The results were not explained by variations in signal quality, demographics or acquisition methods. These findings provide a quantitative framework capturing the diversity of accelerated brain aging.

The brain undergoes dynamic functional changes with age[1–3]. Accurately mapping the trajectory of these changes and how they relate to chronological age is critical for understanding the aging process, multilevel disparities[4,5] and brain disorders[1] such as the Alzheimer's disease continuum, which includes mild cognitive impairment (MCI) and related disorders like behavioral variant frontotemporal dementia (bvFTD)[6]. Brain clocks or brain-age models have emerged as dimensional, transdiagnostic metrics that measure brain health influenced by a range of factors[7–9], suggesting that they may be able to capture multimodal diversity[10]. Populations from LAC exhibit higher genetic diversity and distinct physical, social and internal exposomes[11,12] that impact brain phenotypes[4,13,14]. Income and socioeconomic inequality[15,16], high levels of air pollution[17], limited access to timely and effective healthcare[18], rising prevalence of communicable and noncommunicable diseases[19,20], and low education attainment[21,22] are determinants of brain health in LAC[18]. Thus, although measuring the brain-age gap could enhance our understanding of disease risk and its impact on accelerated aging[23], there is a lack of research on brain-age models

e-mail: agustin.ibanez@gbhi.org

https://doi.org/10.1038/s41591-024-03209-x

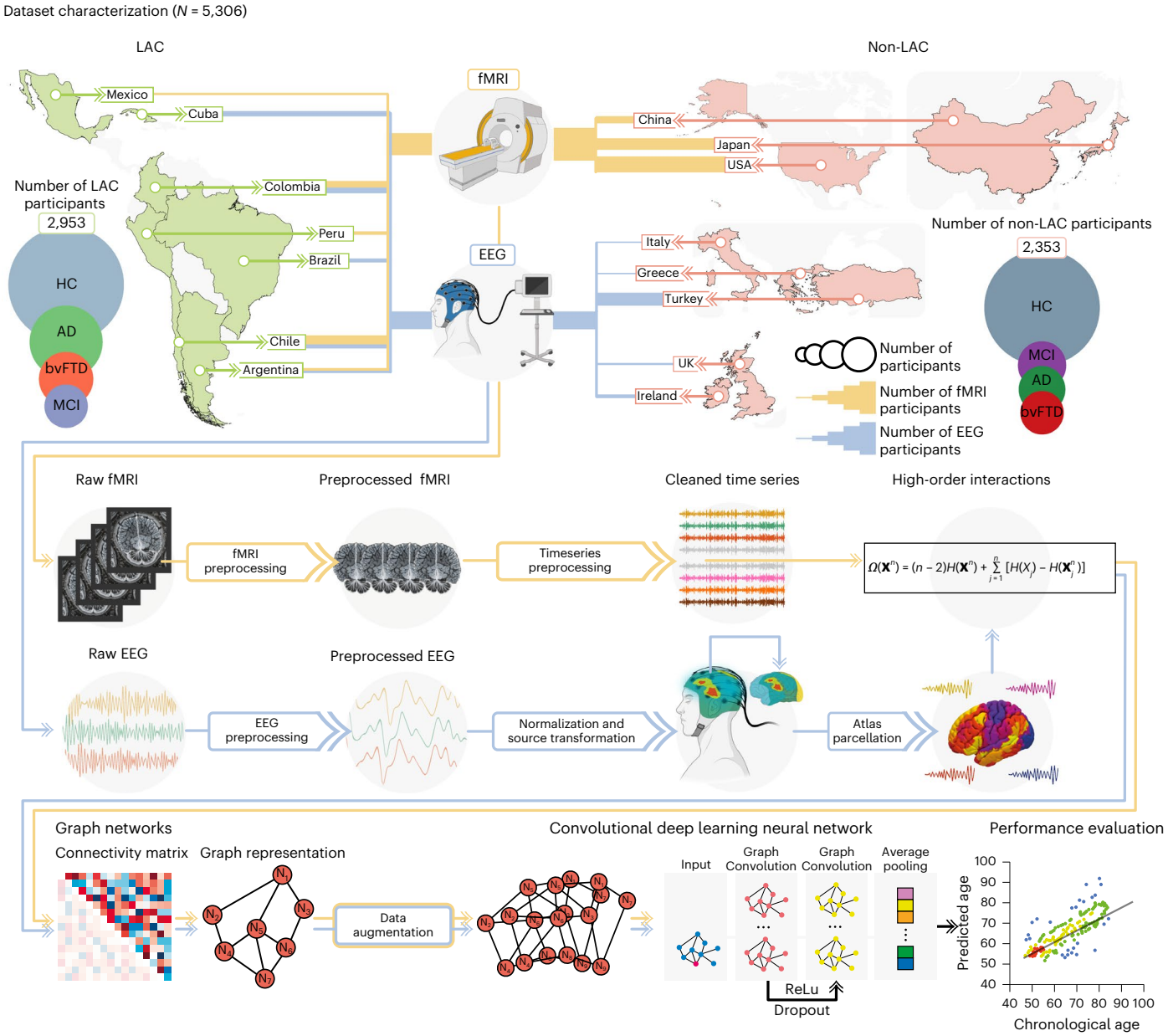

Fig. 1 | Dataset characterization and analysis pipeline. Datasets included LAC and non-LAC healthy controls (HC, total $n = 3,509$) and participants with Alzheimer disease (AD, total $n = 828$), bvFTD (total $n = 463$) and MCI (total $n = 517$). The fMRI dataset included 2,953 participants from LAC (Argentina, Chile, Colombia, Mexico and Peru) as well as non-LAC (the USA, China and Japan). The EEG dataset involved 2,353 participants from Argentina, Brazil, Chile, Colombia and Cuba (LAC) as well as Greece, Ireland, Italy, Turkey and the UK (non-LAC). The raw fMRI and EEG signals were preprocessed by filtering and artifact removal and the EEG signals were normalized to project them into source space. A parcellation using the automated anatomical labeling (AAL) atlas for both the fMRI and EEG signals was performed to build the nodes from which we calculated the high-order interactions using the Ω-information metric. A connectivity matrix was obtained for both modalities, which was later represented by graphs. Data augmentation was performed only in the testing dataset. The graphs were used as input for a graph convolutional deep learning network (architecture shown in the last row), with separate models for EEG and fMRI. Finally, age prediction was obtained, and the performance was measured by comparing the predicted versus the chronological ages. This figure was partially created with BioRender.com (fMRI and EEG devices).

in underrepresented populations where they experience large socio-economic and health disparities[18,24,25].

Sex and gender differences emerge as critical factors influencing brain changes. Studies on atrophy in the Alzheimer disease continuum reveal a faster rate of brain atrophy in females than in males[26]. Moreover, country-level gender inequality is associated with sex differences in cortical thickness[27]. Structural gender inequality further impacts brain health, with adverse environments affecting dendritic branching and synapse formation[28]. However, no studies to date have explored the spectrum of brain-age abnormalities, including the effects of demographic heterogeneity across geographical regions, between sexes, and the continuum from brain health to disease. Further, most studies have been conducted with participants from the Global North, resulting in a lack of generalization to underrepresented populations from the Global South including LAC[24,29–31].

Multimodal machine learning studies show promise in brain aging[23]; however, most rely on structural magnetic resonance imaging (MRI), overlooking brain network dynamics. Complex spatiotemporal dimensions can be tracked with spatial accuracy through functional magnetic resonance imaging (fMRI) and with millisecond precision

using an electroencephalogram (EEG)[32]. Given the complementary strengths of fMRI and EEG, it is crucial to cross-validate existing brain clock models using these techniques. However, no studies have simultaneously applied EEG and fMRI to replicate brain-age effects. In addition, standard machine learning approaches are less generalizable than deep learning methods[33]. Brain-age indices have been restricted by the predominant use of MRI or positron emission tomography, which are less accessible and affordable in LAC, leading to selection biases[34]. EEG offers a solution because of its cost-effectiveness, portability and ease of implementation in aging and dementia[35,36]. However, few studies have combined accessible techniques with deep learning to develop scalable brain-age markers. The application of EEG is hindered by heterogeneity in recordings, electrode layouts, acquisition systems, processing pipelines and small sample sizes[37]. These standardization challenges have impeded the integration of fMRI and EEG in extensive, multicenter brain-age research.

We adopted a framework to tackle diversity by including datasets from LAC and non-LAC regions, utilizing graph convolutional networks (GCN) to functional connectivity of fMRI and EEG signals. We hypothesized that, across fMRI and EEG imaging, models would accurately predict brain-age gaps and be sensitive to the impacts of multimodal diversity, including geographical and sociodemographic effects, sex differences, health disparities and exposome influences. By testing this hypothesis, we aimed to assess the effectiveness of high-order interactions and deep learning in predicting brain-age differences across diverse and heterogeneous populations of healthy aging and neurocognitive disorders.

Results

We used resting-state fMRI and EEG signals separately to evaluate whether a deep learning computational pipeline (Fig. 1) captures differences in brain aging across heterogeneous populations from a total of 5,306 datasets. We included fMRI data from 2,953 participants from Argentina, Chile, Colombia, Mexico and Peru (LAC) and the USA, China and Japan (non-LAC). The EEG dataset involved 2,353 participants from Argentina, Brazil, Chile, Colombia and Cuba (LAC), and Greece, Ireland, Italy, Turkey and the UK (non-LAC). Healthy controls, MCI, Alzheimer disease and bvFTD groups were included. We focused on the Alzheimer disease and bvFTD because these conditions represent the most common late-onset and early-onset causes of dementia[38,39]. We included the Alzheimer's disease continuum, which encompasses MCI, to capture the prodromal stages of the disease[39]. Raw fMRI and EEG signals were preprocessed to remove artifacts and then normalized. Based on multivariate information theory, we calculated high-order interactions[1]. Weighted graphs were used as inputs for a graph convolutional deep learning network trained to predict brain age, using one model for fMRI and another for EEG.

Brain-age gap across LAC and non-LAC datasets

We used the fMRI and EEG signals from the control's datasets (LAC and non-LAC) to train and test brain-aging models. We used 80% cross-validation with a 20% hold-out testing split. As shown in Figs. 2a and 3a, our models predicting brain age obtained adequate goodness of fit (fMRI: $R^2 = 0.52$, $P < 0.001$, $f^2 = 1.07$; EEG: $R^2 = 0.45$, $P < 0.001$, $f^2 = 0.83$). We implemented the r.m.s.e. to evaluate models' fit, obtaining acceptable brain-age predictions (fMRI-r.m.s.e. = 7.24, EEG-r.m.s.e. = 6.45). For both, fMRI and EEG, the main predictive brain-regional features included hubs in frontoposterior networks (nodes in precentral gyrus, the middle occipital gyrus, and the superior and middle frontal gyri; Figs. 2a and 3a). Additional nodes for the fMRI model included the inferior frontal gyri, and the anterior and median cingulate and paracingulate gyri (Fig. 2a.). For EEG, key nodes also comprised the superior and inferior parietal gyri and the inferior occipital gyrus (Fig. 3a). Thus, for both fMRI and EEG the models showed an adequate fit and predictive performance, with key predictive features involving frontoposterior networks in the brain.

Brain-age gap in non-LAC datasets

Using the same data split ratio, we trained and tested the models in non-LAC datasets. As shown in Figs. 2b and 3b, our models predicting brain age yielded considerable goodness of fit (fMRI: $R^2 = 0.40$, $P < 0.001$, $f^2 = 0.67$; EEG: $R^2 = 0.43$, $P < 0.001$, $f^2 = 0.76$). The r.m.s.e. values were also adequate (fMRI-r.m.s.e. = 8.66; EEG-r.m.s.e. = 6.54). Mean directional errors (MDE) for fMRI and EEG were 0.69 and 1.07, respectively. For both fMRI and EEG, the main predictive features were hubs in frontoposterior networks including the superior frontal gyrus (dorsolateral), the precentral gyrus and the middle occipital gyrus (Figs. 2b and 3b). Additional critical nodes for the fMRI model included the inferior and middle frontal gyri, and the anterior and median cingulate and paracingulate gyri (Fig. 2b). For EEG, key nodes also comprised the superior and inferior occipital gyri, and the superior parietal gyrus (Fig. 3b). In brief, models trained on non-LAC datasets exhibited strong fit values and predictive features as in the overall dataset analysis.

Brain-age gap in LAC datasets

When trained and tested in the LAC datasets (Figs. 2c and 3c), models demonstrated moderate goodness of fit indexes but were less precise, as indicated by higher r.m.s.e. values (fMRI = 11.91; EEG = 9.82). We observed increased positive biases in the MDE measures compared with the non-LAC models (fMRI = 3.18; EEG = 5.34). Again, the main

Fig. 2 | fMRI training and testing the deep learning model in different datasets. a, Ordinary least squares (OLS) regression comparing chronological age versus predicted age with the feature importance list for training ($n = 1{,}155$) and testing ($n = 289$) in the whole sample ($P < 1 \times 10^{-15}$). **b**, Regression comparing chronological age versus predicted age with the feature importance list for training ($n = 773$) and testing ($n = 194$) in the non-LAC dataset ($P < 1 \times 10^{-15}$). **c**, Regression comparing chronological age versus predicted age with the feature importance list for training ($n = 381$) and testing ($n = 91$) in the LAC dataset ($P = 4.91 \times 10^{-7}$). For **a**, **b** and **c**, the bars show the brain region feature importance list in descending order, with ring plots and glass brain representations of the most important network-edge connections. Feature importance (top 10) data are presented as mean values and 99% CI. The values for the features (mean, left limit, right limit) are: feature 1 = (0.975, 0.952, 0.999), feature 2 = (0.735, 0.715, 0.756), feature 3 = (0.627, 0.597, 0.656), feature 4 = (0.470, 0.449, 0.490), feature 5 = (0.375, 0.353, 0.397), feature 6 = (0.314, 0.285, 0.342), feature 7 = (0.239, 0.217, 0.262), feature 8 = (0.198, 0.169, 0.228), feature 9 = (0.161, 0.128, 0.193), feature 10 = (0.119, 0.093, 0.145) (**a**); feature 1 = (0.968, 0.937, 0.999), feature 2 = (0.736, 0.707, 0.764), feature 3 = (0.541, 0.518, 0.565), feature 4 = (0.434, 0.403, 0.464), feature 5 = (0.315, 0.290, 0.339), feature 6 = (0.253, 0.220, 0.286), feature 7 = (0.177, 0.156, 0.197), feature 8 = (0.140, 0.114, 0.166), feature 9 = (0.111, 0.078, 0.144), feature 10 = (0.079, 0.053, 0.106) (**b**); and feature 1 = (0.971, 0.944, 0.999), feature 2 = (0.847, 0.816, 0.878), feature 3 = (0.698, 0.667, 0.730), feature 4 = (0.533, 0.512, 0.555), feature 5 = (0.458, 0.430, 0.487), feature 6 = (0.371, 0.344, 0.399), feature 7 = (0.298, 0.272, 0.325), feature 8 = (0.242, 0.216, 0.269), feature 9 = (0.198, 0.169, 0.227), feature 10 = (0.163, 0.130, 0.196) (**c**). **d**, Histogram of the prediction error when training in non-LAC dataset (n = 967) and testing in LAC dataset (n = 477). **e**, Violin plot of the distribution and statistical comparison of training and testing with different regions using a two-sided permutation test without multiple comparisons (5,000 algorithm iterations) with a result of $P < 1 \times 10^{-15}$. Mean, first quartile (q1), third quartile (q3), whisker low, whisker high, minima and maxima values for violin plots are: LAC/non-LAC (−2.52, −7.74, 3.31, −22.52, 17.33, −22.52, 17.33); non-LAC/LAC (5.60, 0.85, 12.14, −12.82, 27.75, −12.82, 27.75). **f**, Violin plot of the distribution and statistical comparison of testing the models on females ($n = 261$) and males ($n = 216$) in LAC using a permutation test (5,000 iterations) with a result of $P = 0.042$. Mean, q1, q3, whisker low, whisker high, minima and maxima values for violin plots are: male (3.66, −1.83, 9.45, −12.49, 16.32, −12.49, 16.32); and female (6.93, 2.21, 12.78, −12.82, 27.75, −12.82, 27.75). ROI, region of interest. This figure was partially created with BioRender.com (fMRI device).

https://doi.org/10.1038/s41591-024-03209-x

features involved frontoposterior networks. Common nodes for fMRI and EEG included the superior and middle occipital gyri, the superior and inferior parietal gyri, and the superior and middle frontal gyri (Figs. 2c and 3c). For EEG, the model also highlighted the precentral gyrus and the inferior occipital gyrus (Fig. 3c). Thus, models trained on LAC datasets showed moderate fit and positive biases (older brain age) in frontotemporal nodes (fMRI and EEG), compared with non-LAC models.

fMRI

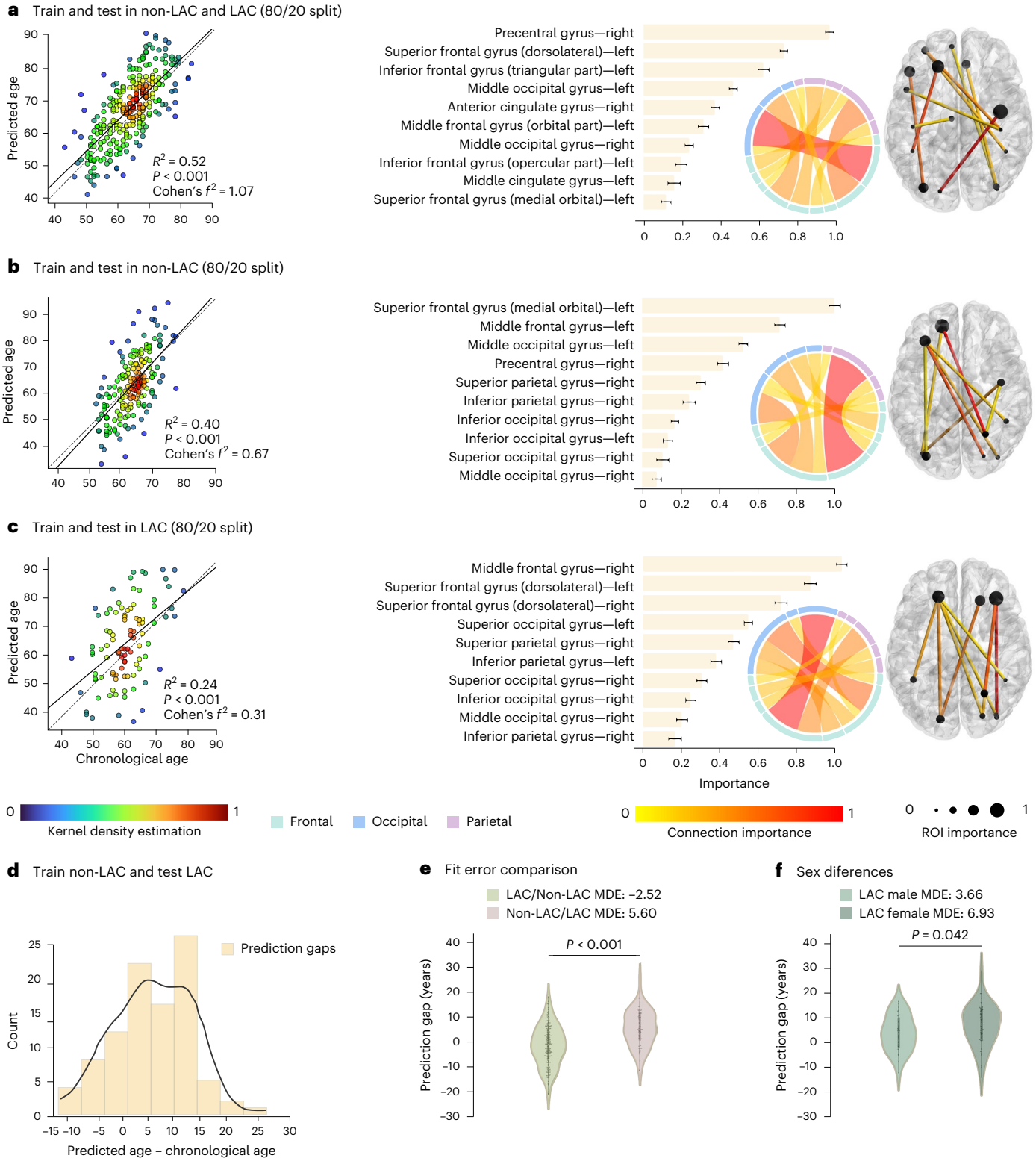

Cross-regional effects in model generalization

We investigated the effects of cross-region training and testing with data from non-LAC and LAC. Training with non-LAC data and testing on LAC data led to biases in predicting older brain ages than the respective chronological ages as shown by positive MDE values (Figs. 2d and 3d; fMRI: MDE = 5.60, r.m.s.e. = 9.44; EEG: MDE = 5.24, r.m.s.e. = 7.23). By contrast, training on LAC and testing on non-LAC resulted in negative age biases predicting younger brain age shown by the MDE (Figs. 2d and 3d; LAC/non-LAC fMRI: MDE = −2.52, r.m.s.e. = 8.41; LAC/non-LAC EEG: MDE = −2.34, r.m.s.e. = 5.69). Sex differences were observed in the brain-age gaps when training in the non-LAC and testing in LAC (Fig. 4a,b). Specifically, female participants in LAC exhibited a greater bias towards older brain age than males (fMRI: $P = 0.04$; EEG: $P = 0.03$). In conclusion, training with non-LAC data and testing on LAC data resulted in a bias towards predicting older brain ages, especially for female participants in LAC.

Accelerated aging in MCI, Alzheimer disease and bvFTD

We investigated the effects of testing the controls-trained model (80%) on different subsamples across the different neurocognitive health and disease spectrum (controls non-LAC, controls LAC, MCI, Alzheimer disease and bvFTD) (Table 1), matched by age, sex and education. Permutation subsample analyses with 5,000 iterations revealed statistically significant brain-age gaps between the non-LAC and LAC control groups (Figs. 4a,b; fMRI: $P < 0.01$; EEG: $P < 1 \times 10^{-5}$). This difference was also observed for Alzheimer disease in the fMRI dataset ($P < 1 \times 10^{-5}$). In addition, for fMRI, we found significant differences between controls from non-LAC and all clinical groups from the same region (MCI ($P < 1 \times 10^{-5}$), Alzheimer disease ($P < 1 \times 10^{-5}$) and bvFTD ($P < 1 \times 10^{-5}$)). Similarly, for both fMRI and EEG, we observed significant differences between controls from LAC and all the clinical groups (fMRI: MCI ($P < 1 \times 10^{-5}$), Alzheimer disease ($P < 1 \times 10^{-5}$) and bvFTD ($P < 1 \times 10^{-5}$); EEG: MCI ($P < 1 \times 10^{-5}$), Alzheimer disease ($P < 1 \times 10^{-5}$) and bvFTD ($P < 0.01$)). Across fMRI and EEG datasetsf, both LAC and non-LAC, we observed a gradient of increasing brain age from controls to MCI to Alzheimer disease. The MCI groups from LAC and non-LAC significantly differed from Alzheimer disease (fMRI and EEG: $P < 1 \times 10^{-5}$) and bvFTD (fMRI: $P < 1 \times 10^{-5}$; EEG: $P < 0.01$) in the respective regions, with older brain ages for Alzheimer disease and bvFTD. For the fMRI and EEG non-LAC datasets, the Alzheimer disease group also showed an older brain age than the bvFTD group ($P < 0.01$). Thus, larger brain-age gaps were observed in LAC compared with non-LAC groups and across clinical groups, with ascending brain age from controls to MCI to dementia.

Sex differences in neurocognitive disorders

For fMRI, we analyzed the differences between male and female participants with the same diagnosis for the non-LAC and LAC datasets. There were no significant differences among groups from non-LAC datasets (Fig. 4a,b). However, females with Alzheimer disease from LAC exhibited significantly greater brain-age gaps compared with the respective males (fMRI: $P < 1 \times 10^{-3}$; EEG: $P < 0.001$). No other effects were observed. We conducted a supplementary analysis incorporating country-level gender inequality indexes (GII), sex, region (LAC versus non-LAC) and individual neurocognitive status (healthy controls versus MCI, Alzheimer disease or bvFTD) as predictors of brain-age gaps. The model demonstrated good performance ($R^2 = 0.40$, $F^2 = 0.66$, r.m.s.e. = 6.85, $P < 1 \times 10^{-15}$) and all predictors were influential. We found that female participants with a neurocognitive disorder living in countries with high gender inequality—particularly from LAC—were associated with higher brain-age gaps (Extended Data Fig. 1 and Supplementary Table 1). Overall, females with Alzheimer disease from LAC exhibited significantly greater brain-age gaps compared with males, influenced by high gender inequality in their countries.

Factors associated with brain-age gap

We used gradient-boosting regression models to explore the influence of physical and social factors, as well as factors of disease disparities on the brain-age gap. Predictors included aggregate country-level measures of air pollution (PM2.5), socioeconomic inequality (Gini index) and burdens of communicable, maternal, prenatal and nutritional conditions, and noncommunicable diseases. We also leveraged the individual neurocognitive status (healthy controls versus Alzheimer disease, MCI or bvFTD). We assessed predictors' importance using a multi-method approach comprising permutation importance, mean decrease in impurity (MDI) and SHapley Additive exPlanations (SHAP) values (Fig. 4c). Across both LAC and non-LAC datasets, the models ($R^2 = 0.41$, $F^2 = 0.71$, r.m.s.e. = 6.76, $F = 304.25$, $P < 1 \times 10^{-15}$) identified neurocognitive disorders (MCI, Alzheimer disease or bvFTD) and higher socioeconomic inequality (Gini index) as the most influential and consistent predictors of increased brain-age gaps (Fig. 4c). High levels of pollution and burden of noncommunicable and communicable diseases were also predictive of increased brain-age gaps, albeit less substantial. Stratified models for LAC ($R^2 = 0.37$, $F^2 = 0.59$, r.m.s.e. = 6.9, $F = 138.78$, $P < 1 \times 10^{-15}$) and non-LAC ($R^2 = 0.41$, $F^2 = 0.71$, r.m.s.e. = 6.57, $F = 135.91$, $P < 1 \times 10^{-15}$) also showed good performance, with neurocognitive disorders being the most influential predictor in both. In LAC, higher socioeconomic inequality was the second most consistent and influential predictor of larger brain-age gaps across the three models. Air pollution and burden of communicable and noncommunicable

Fig. 3 | EEG training and testing the deep learning model in different samples. a, OLS regression comparing chronological age versus predicted age with the feature importance list for training ($n = 1{,}644$) and testing ($n = 411$) in the whole sample ($P < 1 \times 10^{-15}$). **b**, Regression comparing chronological age versus predicted age with the feature importance list for training ($n = 471$) and testing ($n = 118$) in the non-LAC dataset ($P < 1 \times 10^{-15}$). **c**, Regression comparing chronological age versus predicted age with the feature importance list for training ($n = 1{,}188$) and testing ($n = 298$) in the LAC dataset ($P = 3.51 \times 10^{-7}$). For **a**, **b** and **c**, the bars show the brain region feature importance list in descending order, with ring plots and glass brain representations of the most important network-edge connections. Feature importance (top 10) data are presented as mean values and 99% CI. The values for the features (mean, left limit, right limit) are: feature 1 = (0.968, 0.946, 0.991), feature 2 = (0.759, 0.739, 0.779), feature 3 = (0.644, 0.617, 0.670), feature 4 = (0.531, 0.500, 0.561), feature 5 = (0.410, 0.384, 0.436), feature 6 = (0.336, 0.309, 0.363), feature 7 = (0.259, 0.239, 0.279), feature 8 = (0.218, 0.191, 0.245), feature 9 = (0.184, 0.150, 0.217), feature 10 = (0.146, 0.114, 0.177) (**a**); feature 1 = (0.967, 0.935, 0.999), feature 2 = (0.764, 0.741, 0.786), feature 3 = (0.569, 0.549, 0.590), feature 4 = (0.460, 0.435, 0.485), feature 5 = (0.354, 0.330, 0.377), feature 6 = (0.283, 0.256, 0.311), feature 7 = (0.216, 0.192, 0.241), feature 8 = (0.169, 0.145, 0.193), feature 9 = (0.129, 0.107, 0.150), feature 10 = (0.101, 0.077, 0.124) (**b**); feature 1 = (0.972, 0.949, 0.995), feature 2 = (0.833, 0.805, 0.860), feature 3 = (0.705, 0.677, 0.733), feature 4 = (0.564, 0.543, 0.584), feature 5 = (0.488, 0.463, 0.514), feature 6 = (0.408, 0.385, 0.431), feature 7 = (0.363, 0.334, 0.393), feature 8 = (0.292, 0.269, 0.314), feature 9 = (0.243, 0.222, 0.264), feature 10 = (0.221, 0.188, 0.254) (c). **d**, Histogram of the prediction error when training in non-LAC dataset ($n = 569$) and testing in LAC dataset ($n = 1{,}486$). **e**, Violin plot of the distribution and statistical comparison of training and testing with different regions using a two-sided permutation test without multiple comparisons (5,000 algorithm iterations) with a result of $P < 1 \times 10^{-15}$. Mean, q1, q3, whisker low, whisker high, minima and maxima values for violin plots are: LAC/non-LAC (−2.34, −6.07, 1.26, −13.25, 11.52, −20.08, 17.52); non-LAC/LAC (5.24, 1.95, 8.61, −5.24, 16.18, −12.73, 16.18). **f**, Violin plot of the distribution and statistical comparison of testing the models on females and males using a permutation test (5,000 iterations) with a result of $P = 0.012$. Mean, q1, q3, whisker low and whisker high values for violin plots are: male (3.66, 1.87, 7.83, −5.24, 16.18, −12.73, 16.18); female (6.19, 2.67, 9.39, −3.08, 15.52, −3.08, 15.52). This figure was partially created with BioRender.com (EEG device).

https://doi.org/10.1038/s41591-024-03209-x

diseases were also influential. None of these variables were influential predictors in the non-LAC models. Predictors' estimation coefficients are presented in Supplementary Table 2. In sum, neurocognitive disorders, followed by macrosocial factors linked to socioeconomic inequality, air pollution and health disparities were influential predictors of increased brain-age gaps, especially in LAC.

a Train and test in non-LAC and LAC (80/20 split)

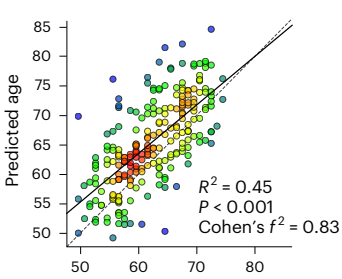

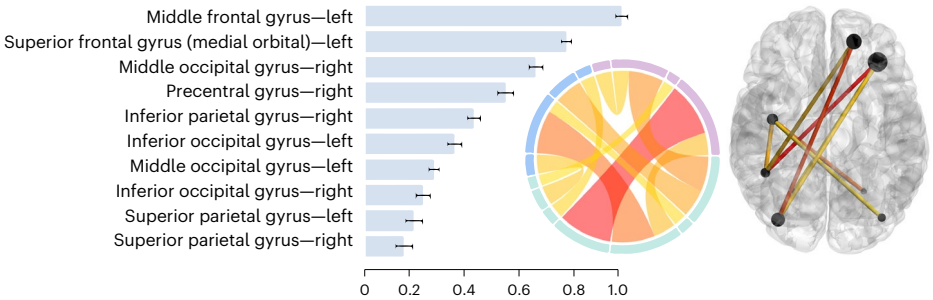

b Train and test in non-LAC (80/20 split)

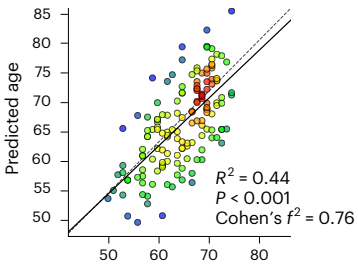

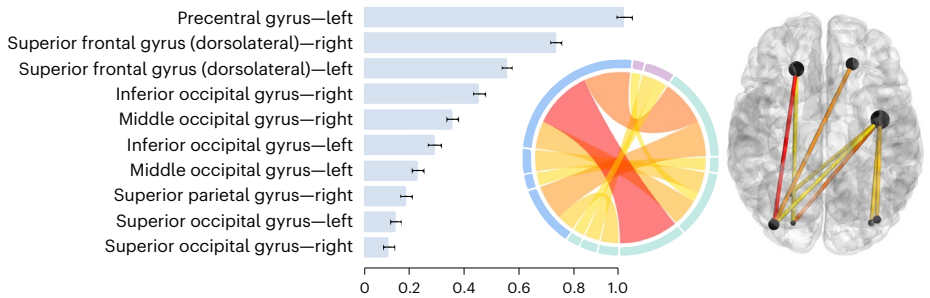

c Train and test in LAC (80/20 split)

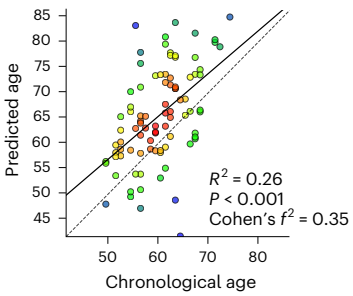

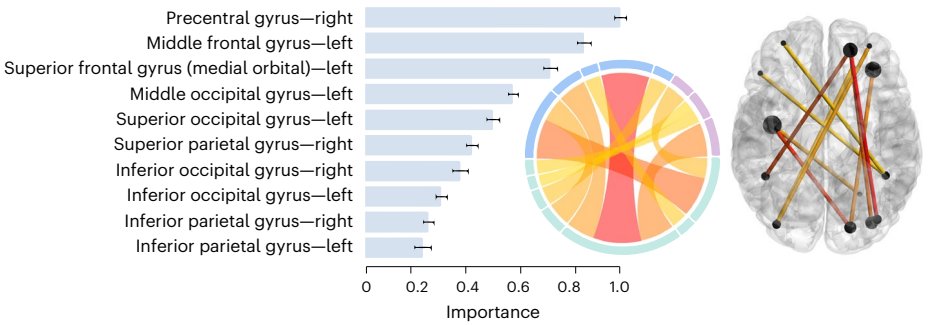

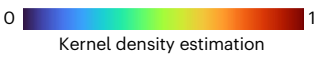

d Train non-LAC and test LAC

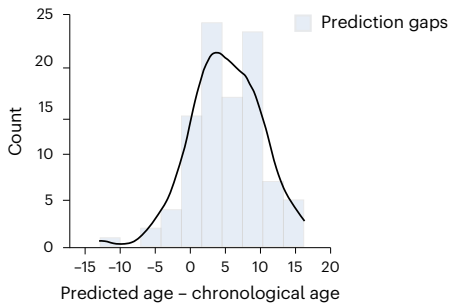

e Fit error comparison

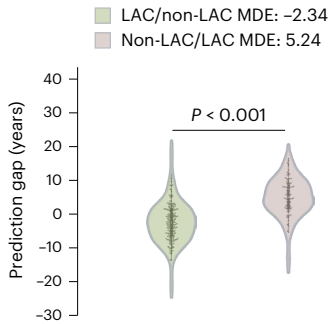

f Sex differences

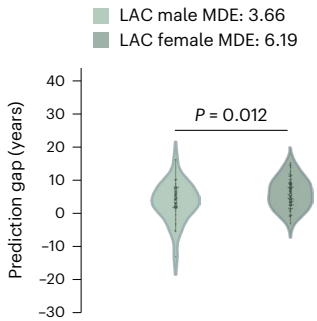

https://doi.org/10.1038/s41591-024-03209-x

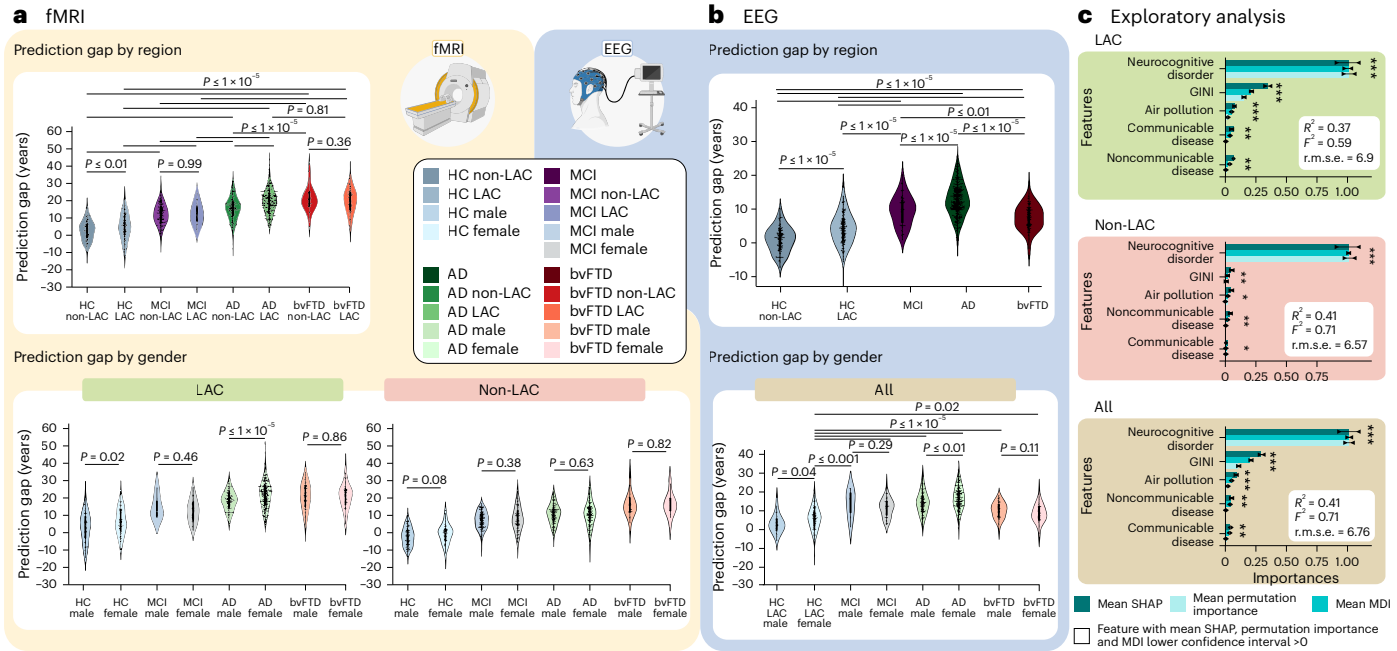

Fig. 4 | Groups, sex and macrosocial influences in brain-age gaps. a,**b**, Violin plots for the distribution of prediction gaps for different groups and sex effects using (**a**) fMRI and (**b**) EEG datasets. Statistical comparisons were calculated using two-sided subsample permutation testing without multiple comparisons and with 5,000 algorithm iterations. **c**, Associations between macrosocial and disease disparity factors with brain-age gaps were assessed with a multi-method approach comprising SHAP values, feature importance (MDI) and permutation importance. Plots show the mean importance values for each method, along with their 99% CI, as well as the average R^2 and Cohen's f^2. *Features whose lower CI boundary does not cross zero. Shaded bars indicate significance across the three methods. We conducted a two-sided *F*-test to evaluate the overall significance of the regression models. The three models were significant: healthy controls LAC ($R^2 = 0.37$ (99% CI ±0.17), $F^2 = 0.59$ (99% CI ±0.21), r.m.s.e. = 6.9 (99% CI ±0.92), $F = 138.78$ ($P < 1 \times 10^{-15}$)); healthy controls non-LAC ($R^2 = 0.41$ (99% CI ±0.17), $F^2 = 0.71$ (99% CI ±0.21), r.m.s.e. = 6.57 (99% CI ±1.31), $F = 135.91$ ($P < 1 \times 10^{-15}$)) and total dataset ($R^2 = 0.41$ (99% CI ±0.12), $F^2 = 0.71$ (99% CI ±0.14), r.m.s.e. = 6.76 (99% CI ±0.89), $F = 253.39$ ($P < 1 \times 10^{-15}$)). The relevance of the features and their respective CI values are available in Supplementary Table 2. F, females; HC LAC, healthy controls from LAC; HC non-LAC, healthy controls from non-LAC; M, males. This figure was partially created with BioRender.com (fMRI and EEG devices).

Sensitivity analyses

We performed multiple tests to assess the validity of the results. First, we investigated whether variations in fMRI or EEG data quality explained the differences in brain age between the non-LAC and LAC. Subsample permutation tests with 5,000 iterations showed no differences between any of the groups for fMRI (Fig. 5a) or EEG (Fig. 5b) data quality metrics. In addition, a linear regression examining scanner-type effects showed that the fMRI data quality metric did not predict the brain-age gaps ($R^2 = 0.001$, $P = 0.18$, Cohen's $f^2 = 0.001$, Fig. 5c). To further test for scanner effects, we implemented a harmonization strategy by normalizing the brain-age gap variable within each scanner type. We used the min–max scaler to ensure consistent minimum and maximum values across scanners. Results using this harmonization (Fig. 5d) and our initial approach were very similar. Additional analyses controlling for datasets collected with eyes open versus eyes closed protocols revealed no significant differences in brain-age gaps across any groups (Extended Data Fig. 2).

We also controlled for the effects of age and years of education on the brain-age gap from fMRI and EEG by including them as covariates in the group comparisons. All reported group differences remained significant after covariate adjustment (Supplementary Table 3). Years of education did not change the results for any analyses. In eight of the nine analyses, age did not have a significant effect. Considering the chronological age differences between the Alzheimer disease and MCI groups, we performed a sensitivity analysis using a subset of participants with MCI (fMRI: $n = 254$, mean age = 73.287 ± 7.517 years; EEG: $n = 52$, mean age = 63.231 ± 6.549 years) age matched to participants with Alzheimer disease (fMRI: $n = 254$, mean age = 72.295 ± 7.530 years, $P = 0.13$; EEG: $n = 52$, mean age = 62.769 ± 6.302 years, $P = 0.71$). These results (Extended Data Fig. 3) confirmed those reported for the overall MCI and Alzheimer disease datasets (Fig. 4a,b). For both fMRI and EEG datasets, we found significantly larger brain-age gaps in Alzheimer disease compared with MCI (fMRI: $P < 1 \times 10^{-5}$; EEG: $P < 0.01$). For fMRI, these differences were observed in both LAC ($P < 1 \times 10^{-5}$) and non-LAC ($P < 1 \times 10^{-5}$) datasets. We also found differences between participants with MCI from LAC versus non-LAC ($P < 1 \times 10^{-5}$) and participants with Alzheimer disease from LAC versus non-LAC ($P < 1 \times 10^{-5}$). Thus, controlling for data quality, scanner effects, age and education confirmed that the reported effects in brain-age gaps remained the same.

Discussion

Our study used brain clocks to capture the diversity and disparities across LAC and non-LAC datasets using fMRI and source space EEG techniques. Despite heterogeneity in signal acquisition and methods, we captured patterns of brain-age modulations in healthy aging from diverse datasets and participants with MCI, Alzheimer disease and bvFTD. Models trained and tested on non-LAC datasets showed greater convergence with chronological age. Conversely, models applied to LAC datasets indicated larger brain-age gaps, suggesting accelerated aging. We observed ascending brain-age gaps from controls to MCI to Alzheimer disease. Sex differences revealed an increased brain-age gap in females in the control and Alzheimer disease groups. Most brain clock patterns were independently confirmed and replicated across fMRI and EEG. Aggregate-level macrosocial factors, including socioeconomic inequality, pollution and burden of communicable/noncommunicable conditions modulated the brain-age gap, especially in LAC. Variations in signal quality, demographics or acquisition methods did not account for the results. The findings offer a framework that captures the multimodal diversity associated with accelerated aging in global settings.

https://doi.org/10.1038/s41591-024-03209-x

Table 1 | Demographics for fMRI and EEG datasets

		HC	MCI	AD	bvFTD	Statistics non-LAC versus LAC	Post hoc comparisons
Full dataset							
All participants (*N*=5,306)		*n*=3,509	*n*=517	*n*=828	*n*=463		
fMRI dataset							
Variable		Non-LAC: *n*=967; LAC: *n*=477	Non-LAC: *n*=215; LAC: *n*=169	Non-LAC: *n*=214; LAC: *n*=505	Non-LAC: *n*=190; LAC *n*=216		
Sex (female:male)	Non-LAC	470:497	114:101	112:102	98:92	χ^2=2.19 *P*=0.533	HC-MCI: *P*=0.453 HC-AD: *P*=0.462 HC-bvFTD: =0.472
	LAC	261:216	84:85	262:243	105:111	χ^2=2.76 *P*=0.429	HC-MCI: *P*=0.438 HC-AD: *P*=0.447 HC-bvFTD: *P*=0.459
Age (years) (range: 22–91)	Non-LAC	53.55 (13.43)	59.62 (8.77)	76.59 (9.35)	73.14 (8.56)	*F*=3.13 *P*=0.47 ηp^2=0.02	HC-MCI: *P*=0.443 HC-AD: *P*=0.451 HC-bvFTD: *P*=0.461
	LAC	65.34 (11.44)	66.53 (8.18)	77.52 (9.35)	73.15 (8.76)	*F*=3.62 *P*=0.45 ηp^2=0.02	HC-MCI: *P*=0.39 HC-AD: *P*=0.41 HC-bvFTD: *P*=0.461
Years of education (range: 0–25)	Non-LAC	13.15 (5.41)	14.15 (3.41)	13.12 (5.34)	11.16 (3.56)	*F*=2.19 *P*=0.49 ηp^2=0.02	HC-MCI: *P*=0.472 HC-AD: *P*=0.484 HC-bvFTD: *P*=0.491
	LAC	12.11 (3.39)	11.52 (6.32)	8.89 (4.34)	7.89 (3.36)	*F*=1.31 *P*=0.68 ηp^2=0.01	HC-MCI: *P*=0.672 HC-AD: *P*=0.681 HC-bvFTD: *P*=0.654
EEG dataset							
		Non-LAC *n*=569; LAC *n*=1,486	LAC *n*=133	LAC *n*=108	LAC *n*=57		
Sex (female:male)	Non-LAC	470:99	—	—	—	χ^2=64.62 $P=1\times10^{-15}$	—
	LAC	954:532	111:22	85:23	39:18	χ^2=28.05 *P*=0.000003	HC-MCI: *P*=0.063 HC-AD: *P*=0.071 HC-bvFTD: *P*=0.075
Age (years) (range: 21–92)	Non-LAC	58.98 (12.03)	—	—	—	*t*=4.21 *P*=0.07 ηp^2=0.02	—
	LAC	66.74 (13.94)	62.54 (9.98)	78.62 (8.34)	71.05 (9.34)	*F*=7.62 *P*=0.0005 ηp^2=0.07	HC-MCI: *P*=0.052 HC-AD: *P*=0.061 HC-bvFTD: *P*=0.067
Years of education (range: 0–24)	Non-LAC	14.85 (4.91)	—	—	—	*t*=3.54 *P*=0.08 ηp^2=0.01	—
	LAC	13.92 (3.39)	8.12 (4.34)	10.75 (6.32)	14.38 (5.49)	*F*=6.31 *P*=0.0007 ηp^2=0.06	HC-MCI: *P*=0.058 HC-AD: *P*=0.063 HC-bvFTD: *P*=0.069

Results are presented as mean (s.d.). Demographic data comparing non-LAC and LAC groups were assessed using unpaired two-sided *t*-tests, whereas data for pathological groups were analyzed using right-sided analyses of variance followed by Tukey post-hoc pairwise comparisons, except for sex, which was analyzed using two-sided Pearson's chi-squared (χ^2) test. Effect sizes were calculated using partial eta squared (ηp^2). AD, Alzheimer disease; *F*, *F*-statistic from ANOVA; *t*, *t*-statistic from *t*-test.

Our results suggest that being from LAC is associated with accelerated aging. The better fit of the non-LAC compared to the LAC models supports the notion that universal models of brain phenotypes do not generalize well to underrepresented populations[24,29,40]. Diversity-related factors associated with different exposures and disease outcomes[4,10,24,41] may influence the brain-age gaps in LAC and non-LAC. Neurocognitive disorders played a crucial role[4,42]. However, structural socioeconomic inequality, a distinctive characteristic of LAC[15], increased levels air pollution[43], and the burden of noncommunicable[19,20] and communicable[18,44] diseases are also important factors on the brain-age gap. The fact that these effects were larger in LAC suggests that underlying inequalities and adverse environmental and health conditions play a macrosocial, structural driving role[11] in the observed regional differences. Immigration may also influence brain age through social determinants of health[45] and genetic diversity. In LAC, tricontinental admixtures lead to substantial ancestral diversity within and across countries[46], impacting dementia prevalence and brain phenotypes[41]. Future studies should consider these potential effects in brain-age gaps.

Selective brain networks were associated with larger brain-age gap in the clinical groups. Both fMRI and EEG models of brain-age gaps yielded large-scale frontoposterior high-order interactions[1], consistent with models of brain age involving long-range connections between frontal, cingular, parietal, and occipital hubs, which may be more vulnerable to aging effects[47–49]. Also consistent with the cumulative nature of neurobiological changes over time[50], brain-age gaps increased from

https://doi.org/10.1038/s41591-024-03209-x

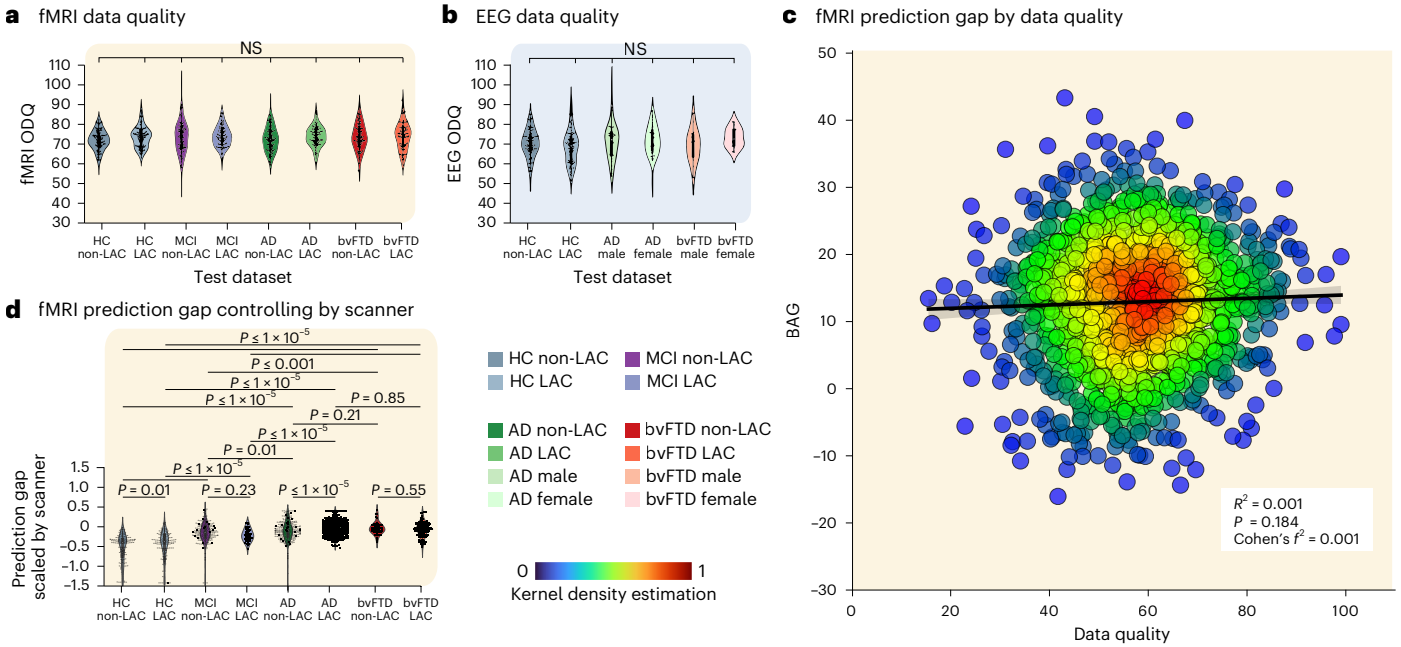

Fig. 5 | Sensitivity analysis. a, Violin plots for the distribution of data quality metrics of fMRI (healthy controls non-LAC, $n = 967$, MCI non-LAC $n = 215$, Alzheimer disease non-LAC $n = 214$, bvFTD non-LAC $n = 190$, HC LAC $n = 477$, MCI LAC $n = 169$, AD LAC $n = 505$, bvFTD LAC $n = 216$). **b**, Violin plots for the distribution of data quality metrics of EEG datasets (HC non-LAC $n = 569$, HC LAC $n = 1486$, MCI LAC $n = 133$, Alzheimer disease LAC $n = 108$, bvFTD LAC $n = 57$). Both **a** and **b** indicate null results between groups in terms of data quality. **c**, Linear regression effects of scanner type, evidencing that the fMRI data quality was not significantly associated with fMRI brain-age gaps differences ($P = 0.184$). **d**, fMRI brain-age gap differences across groups controlling for scanner differences. The statistical comparisons were calculated using two-sided subsample permutation testing with 5,000 iterations. NS, not significant; ODQ, overall data quality.

controls through MCI to Alzheimer disease. A previous deep learning study using MRI and positron emission tomography in participants with MCI and dementia also indicated increased brain-age associated with disease progression[23]. Our results point to the brain age of MCI as being an intermediate stage between healthy aging and dementia[39], and suggest that both fMRI and EEG markers of brain age may help identify groups at greater risk of progressing to dementia.

Sex and gender have been linked to poorer brain health outcomes[27,51]. Larger brain-age gaps in healthy controls and females with Alzheimer disease from LAC may relate to sex-specific conditions such as menopause, which involves brain volume reduction and increased amyloid-beta deposition[52,53]. Females also exhibit a disproportionate tau brain burden[54], pronounced inflammatory dysregulation[55] and lower basal autophagy[56] compared with males, all of which increase Alzheimer disease risk. Such sex-specific factors are intertwined with environmental factors and gender disparities[51]. Females in countries with higher gender inequality exhibit greater cortical atrophy[27]. Our sex effects were specific for Alzheimer disease and LAC, consistent with the impacts of environmental[41] versus genetic risks[57] in Alzheimer disease and bvFTD, respectively. Despite advances in gender equality, women in LAC still face important obstacles[58] including lower education, less income and healthcare access, and greater caregiving burden, potentially exacerbating brain health issues and Alzheimer disease risk[59,60]. Previous models for brain age have been conducted predominantly in high-income settings, ignoring sex and gender differences triggered by region-specific influences[30,31]. Thus, the inclusion of diverse samples can help to better understand the biological and environmental interaction with sex and gender disparities.

Our study had different strengths. We used diverse datasets across LAC and non-LAC including 15 countries, featuring large sample sizes, and replicated results across fMRI and EEG. We used an integrative approach to analyze fMRI and EEG data across a large and geographically diverse sample. The convergence of two neuroimaging techniques and population heterogeneity enhanced the generalizability to the computational models that capture diversity[10]. In particular, incorporating EEG offers affordable and scalable solutions for low-resourced settings, such as those in LAC, compared with traditional neuroimaging techniques[1,35]. Brain clocks based on high-order interactions capture many risks to brain health, and thus, offer an approach to personalized medicine, particularly for underrepresented populations. Our framework combines multiple dimensions of diversity in brain health, the Alzheimer disease continuum and related disorders within a single measure of brain clocks. Accessible metrics of accelerated aging can offer personalized assessments of diversity, aging, and neurocognitive disorders.

This study has multiple limitations. Our EEG dataset lacks representation from clinical groups in non-LAC, which may limit the generalizability. This issue is partially mitigated by the consistent results from the fMRI data, which included MCI, Alzheimer disease and bvFTD groups from LAC and non-LAC regions. Our approach to measure the brain-age gap is unimodal. Future research should adopt multimodal approaches to deepen our understanding of brain aging across different pathophysiological mechanisms[1]. We leveraged two independent training and test datasets with fMRI and EEG, with out-of-sample validation yielding consistent results across geographical comparisons, sex effects and clinical conditions. These datasets involve multimodal settings and recording parameters, suggesting that our results are replicable across highly variable conditions. However, future research should include more regions to further validate our findings. In addition, we did not include individual-level data on gender identity, socioeconomic status and ethnic stratification. Future research incorporating these variables could further enrich our understanding of brain age across diverse populations. Lastly, the sex differences observed between controls from LAC and non-LAC exhibited moderate effect sizes. Further research should assess sex differences in other regions.

In conclusion, brain clock models were sensitive to the impact of diversity involving geographical, sex, macrosocial and disease-based factors from diverse populations, despite the heterogeneity in data

acquisition and processing. Utilizing a deep learning architecture of the brain's high-order interactions[1] across fMRI and EEG signals, combined with globally accessible and affordable data, our study paves the way for more-inclusive tools to assess disparities and diversity in brain aging. These tools can be vital in identifying MCI, Alzheimer disease and bvFTD risk factors, as well as characterizing and staging disease processes. In the future, personalized medicine approaches could leverage models of brain-age gaps to establish worldwide protocols for aging and neurocognitive disorders.

Online content

Any methods, additional references, Nature Portfolio reporting summaries, source data, extended data, supplementary information, acknowledgements, peer review information; details of author contributions and competing interests; and statements of data and code availability are available at https://doi.org/10.1038/s41591-024-03209-x.

References

1. Ibanez, A., Kringelback, M. & Deco, G. A synergetic turn in cognitive neuroscience of brain diseases. *Trends Cogn. Sci.* **28**, 319–338 (2024).
2. Tian, Y. E. et al. Heterogeneous aging across multiple organ systems and prediction of chronic disease and mortality. *Nat. Med.* **29**, 1221–1231 (2023).
3. Hou, Y. et al. Ageing as a risk factor for neurodegenerative disease. *Nat. Rev. Neurol.* **15**, 565–581 (2019).
4. Santamaria-Garcia, H. et al. Factors associated with healthy aging in Latin American populations. *Nat. Med.* **29**, 2248–2258 (2023).
5. Walters, H. Diverse factors shape healthy aging in Latin America. *Nat. Aging* **3**, 1175 (2023).
6. Tseng, W. I., Hsu, Y. C. & Kao, T. W. Brain age difference at baseline predicts clinical dementia rating change in approximately two years. *J. Alzheimers Dis.* **86**, 613–627 (2022).
7. Mukadam, N., Sommerlad, A., Huntley, J. & Livingston, G. Population attributable fractions for risk factors for dementia in low-income and middle-income countries: an analysis using cross-sectional survey data. *Lancet Glob. Health* **7**, e596–e603 (2019).
8. Boyle, P. A. et al. The 'cognitive clock': a novel indicator of brain health. *Alzheimers Dement.* **17**, 1923–1937 (2021).
9. Parra, M. A. et al. Dementia in Latin America: paving the way toward a regional action plan. *Alzheimers Dement.* **17**, 295–313 (2021).
10. Ibanez, A. & Zimmer, E. Time to synergize mental health with brain health. *Nat. Ment. Health* **1**, 441–443 (2023).
11. Ibanez, A. et al. Neuroecological links of the exposome and One Health.*Neuron* **112**, 1905–1910 (2024).
12. Ibanez, A. et al. Healthy aging metanalyses and scoping review of risk factors across Latin America reveal large heterogeneity and weak predictive models. *Nat. Aging* https://doi.org/10.1038/s43587-024-00648-6 (2024).
13. Migeot, J. et al. Allostasis, health, and development in Latin America. *Neurosci. Biobehav. Rev.* **162**, 105697 (2024).
14. Fittipaldi, S. et al. Heterogeneous factors influence social cognition across diverse settings in brain health and age-related diseases. *Nat. Ment. Health* **2**, 63–75 (2024).
15. Gasparini, L. & Cruces, G. *The Changing Picture of Inequality in Latin America: Evidence for Three Decades* (United Nations Development Program, 2022).
16. Chan, M. Y. et al. Socioeconomic status moderates age-related differences in the brain's functional network organization and anatomy across the adult lifespan. *Proc. Natl Acad. Sci. USA* **115**, e5144–e5153 (2018).
17. Fuller, R. et al. Pollution and health: a progress update. *Lancet Planet Health* **6**, e535–e547 (2022).
18. Ibanez, A., Legaz, A. & Ruiz-Adame, M. Addressing the gaps between socioeconomic disparities and biological models of dementia. *Brain* **146**, 3561–3564 (2023).
19. Bilal, U. et al. Life expectancy and mortality in 363 cities of Latin America. *Nat. Med.* **27**, 463–470 (2021).
20. Mullachery, P. H. et al. Mortality amenable to healthcare in Latin American cities: a cross-sectional study examining between-country variation in amenable mortality and the role of urban metrics. *Int. J. Epidemiol.* **51**, 303–313 (2022).
21. Breton, T. R. & Canavire-Bacarreza, G. Low test scores in Latin America: poor schools, poor families or something else? *Compare J. Comp. Int. Educ.* **48**, 733–748 (2018).
22. Gonzalez-Gomez, R. et al. Educational disparities in brain health and dementia across Latin America and the United States. *Alzheimers Dement.* https://doi.org/10.1002/alz.14085 (2024).
23. Lee, J. et al. Deep learning-based brain age prediction in normal aging and dementia. *Nat. Aging* **2**, 412–424 (2022).
24. Baez, S., Alladi, S. & Ibanez, A. Global South research is critical for understanding brain health, ageing and dementia.*Clin. Transl. Med.* **13**, e1486 (2023).
25. Maito, M. A. et al. Classification of Alzheimer's disease and frontotemporal dementia using routine clinical and cognitive measures across multicentric underrepresented samples: a cross sectional observational study. *Lancet Reg. Health Am.* **17**, 100387 (2023).
26. Ardekani, B. A., Convit, A. & Bachman, A. H. Analysis of the MIRIAD data shows sex differences in hippocampal atrophy progression. *J. Alzheimers Dis.* **50**, 847–857 (2016).
27. Zugman, A. et al. Country-level gender inequality is associated with structural differences in the brains of women and men. *Proc. Natl Acad. Sci. USA* **120**, e2218782120 (2023).
28. Nithianantharajah, J. & Hannan, A. J. Enriched environments, experience-dependent plasticity and disorders of the nervous system. *Nat. Rev. Neurosci.* **7**, 697–709 (2006).
29. Greene, A. S. et al. Brain-phenotype models fail for individuals who defy sample stereotypes. *Nature* **609**, 109–118 (2022).
30. Khayretdinova, M. et al. Predicting age from resting-state scalp EEG signals with deep convolutional neural networks on TD-brain dataset. *Front. Aging Neurosci.* **14**, 1019869 (2022).
31. Al Zoubi, O. et al. Predicting age from brain EEG signals—a machine learning approach. *Front. Aging Neurosci.* **10**, 184 (2018).
32. Herzog, R. et al. Genuine high-order interactions in brain networks and neurodegeneration. *Neurobiol. Dis.* **175**, 105918 (2022).
33. Shen, D., Wu, G. & Suk, H. Deep learning in medical image analysis. *Annu. Rev. Biomed. Eng.* **19**, 221–248 (2017).
34. Fry, A. et al. Comparison of sociodemographic and health-related characteristics of UK Biobank participants with those of the general population. *Am. J. Epidemiol.* **186**, 1026–1034 (2017).
35. Hernandez, H. et al. Brain health in diverse settings: how age, demographics and cognition shape brain function. *Neuroimage* **295**, 120636 (2024).
36. Coronel-Oliveros, C. et al. Viscous dynamics associated with hypoexcitation and structural disintegration in neurodegeneration via generative whole-brain modeling. *Alzheimers Dement.* **20**, 3228–3250 (2024).
37. Prado, P. et al. Dementia ConnEEGtome: towards multicentric harmonization of EEG connectivity in neurodegeneration. *Int. J. Psychophysiol.* **172**, 24–38 (2022).
38. Ducharme, S. et al. Recommendations to distinguish behavioural variant frontotemporal dementia from psychiatric disorders. *Brain* **143**, 1632–1650 (2020).
39. Gustavsson, A. et al. Global estimates on the number of persons across the Alzheimer's disease continuum. *Alzheimers Dement.* **19**, 658–670 (2023).

40. Moguilner, S. et al. Biophysical models applied to dementia patients reveal links between geographical origin, gender, disease duration, and loss of neural inhibition. *Alzheimers Res. Ther.* **16**, 79 (2024).
41. Babulal, G. M. et al. Perspectives on ethnic and racial disparities in Alzheimer's disease and related dementias: update and areas of immediate need. *Alzheimers Dement.* **15**, 292–312 (2019).
42. Nianogo, R. A. et al. Risk factors associated with Alzheimer disease and related dementias by sex and race and ethnicity in the US. *JAMA Neurol.* **79**, 584–591 (2022).
43. Gouveia, N. et al. Short-term associations between fine particulate air pollution and cardiovascular and respiratory mortality in 337 cities in Latin America. *Sci. Total Environ.* **920**, 171073 (2024).
44. Hierink, F., Okiro, E. A., Flahault, A. & Ray, N. The winding road to health: a systematic scoping review on the effect of geographical accessibility to health care on infectious diseases in low- and middle-income countries. *PLoS ONE* **16**, e0244921 (2021).
45. Hossin, M. Z. International migration and health: it is time to go beyond conventional theoretical frameworks. *BMJ Glob. Health* **5**, e001938 (2020).
46. Reitz, C., Pericak-Vance, M. A., Foroud, T. & Mayeux, R. A global view of the genetic basis of Alzheimer disease. *Nat. Rev. Neurol.* **19**, 261–277 (2023).
47. Pardo, J. V. et al. Where the brain grows old: decline in anterior cingulate and medial prefrontal function with normal aging. *Neuroimage* **35**, 1231–1237 (2007).
48. Tomasi, D. & Volkow, N. D. Aging and functional brain networks. *Mol. Psychiatry* **17**, 549–458 (2012). 471.
49. Rempe, M. P. et al. Spontaneous cortical dynamics from the first years to the golden years. *Proc. Natl Acad. Sci. USA* **120**, e2212776120 (2023).
50. Hayflick, L. Biological aging is no longer an unsolved problem. *Ann. N. Y. Acad. Sci.* **1**, 1–13 (2007).
51. Mielke, M. M. et al. Consideration of sex and gender in Alzheimer's disease and related disorders from a global perspective. *Alzheimers Dement.* **18**, 2707–2724 (2022).
52. Mosconi, L. et al. Sex differences in Alzheimer risk: brain imaging of endocrine vs chronologic aging. *Neurology* **89**, 1382–1390 (2017).
53. Storsve, A. B. et al. Differential longitudinal changes in cortical thickness, surface area and volume across the adult life span: regions of accelerating and decelerating change. *J. Neurosci.* **34**, 8488–8498 (2014).
54. Snyder, H. M. et al. Sex biology contributions to vulnerability to Alzheimer's disease: a think tank convened by the Women's Alzheimer's Research Initiative. *Alzheimers Dement.* **12**, 1186–1196 (2016).
55. Forsyth, K. S., Jiwrajka, N., Lovell, C. D., Toothacre, N. E. & Anguera, M. C. The conneXion between sex and immune responses. *Nat. Rev. Immunol.* **24**, 487–502 (2024).
56. Congdon, E. E. Sex differences in autophagy contribute to female vulnerability in Alzheimer's disease. *Front. Neurosci.* **12**, 372 (2018).
57. Wood, E. M. et al. Development and validation of pedigree classification criteria for frontotemporal lobar degeneration. *JAMA Neurol.* **70**, 1411–1417 (2013).
58. Medina-Hernández, E., Fernández-Gómez, M. J. & Barrera-Mellado, I. Gender inequality in Latin America: a multidimensional analysis based on ECLAC indicators. *Sustainability* **13**, 13140 (2021).
59. Aranda, M. P. et al. Impact of dementia: health disparities, population trends, care interventions, and economic costs. *J. Am. Geriatr. Soc.* **69**, 1774–1783 (2021).
60. Caldwell, J. Z. K. & Isenberg, N. The aging brain: risk factors and interventions for long term brain health in women. *Curr. Opin. Obstet. Gynecol.* **35**, 169–175 (2023).

Sebastian Moguilner[1,2,3,73], Sandra Baez[4,5,6,73], Hernan Hernandez[1], Joaquín Migeot[1], Agustina Legaz[1,2], Raul Gonzalez-Gomez[1], Francesca R. Farina[5,6,7], Pavel Prado[8], Jhosmary Cuadros[1,9,10], Enzo Tagliazucchi[1,11], Florencia Altschuler[2], Marcelo Adrián Maito[1,2], María E. Godoy[1,2], Josephine Cruzat[1], Pedro A. Valdes-Sosa[12,13,14], Francisco Lopera[15], John Fredy Ochoa-Gómez[15], Alfredis Gonzalez Hernandez[16], Jasmin Bonilla-Santos[17], Rodrigo A. Gonzalez-Montealegre[18], Renato Anghinah[19,20], Luís E. d'Almeida Manfrinati[19,20], Sol Fittipaldi[1,5,6], Vicente Medel[1], Daniela Olivares[1,21,22,23], Görsev G. Yener[24,25,26], Javier Escudero[27], Claudio Babiloni[28,29], Robert Whelan[5,6,30], Bahar Güntekin[31,32,33], Harun Yırıkoğulları[31,32], Hernando Santamaria-Garcia[34,35], Alberto Fernández Lucas[36], David Huepe[21], Gaetano Di Caterina[37], Marcio Soto-Añari[38], Agustina Birba[1], Agustin Sainz-Ballesteros[1], Carlos Coronel-Oliveros[1,5,6,39], Amanuel Yigezu[7], Eduar Herrera[40], Daniel Abasolo[41], Kerry Kilborn[42], Nicolás Rubido[43], Ruaridh A. Clark[44], Ruben Herzog[1,45], Deniz Yerlikaya[46], Kun Hu[47], Mario A. Parra[48,49], Pablo Reyes[34,35], Adolfo M. García[2,5,6,50], Diana L. Matallana[34,35,51], José Alberto Avila-Funes[52], Andrea Slachevsky[53,54,55], María I. Behrens[56,57,58,59], Nilton Custodio[60], Juan F. Cardona[61], Pablo Barttfeld[62], Ignacio L. Brusco[63], Martín A. Bruno[64], Ana L. Sosa Ortiz[65], Stefanie D. Pina-Escudero[5,6,66], Leonel T. Takada[67], Elisa Resende[68], Katherine L. Possin[5,6,66], Maira Okada de Oliveira[5,6,67], Alejandro Lopez-Valdes[5,6,69,70,71], Brian Lawlor[5,6], Ian H. Robertson[5,6,66], Kenneth S. Kosik[72], Claudia Duran-Aniotz[1], Victor Valcour[5,6,66], Jennifer S. Yokoyama[5,6,66], Bruce Miller[5,6,66] & Agustin Ibanez[1,2,5,6] ✉

[1]Latin American Brain Health Institute, Universidad Adolfo Ibañez, Santiago de Chile, Chile. [2]Cognitive Neuroscience Center, Universidad de San Andrés, Buenos Aires, Argentina. [3]Department of Neurology, Massachusetts General Hospital and Harvard Medical School, Boston, MA, USA. [4]Universidad de los Andes, Bogota, Colombia. [5]Global Brain Health Institute (GBHI), University of California, San Francisco, CA, USA. [6]Global Brain Health Institute (GBHI), Trinity College Dublin, Dublin, Ireland. [7]The University of California Santa Barbara (UCSB), Santa Barbara, CA, USA. [8]Escuela de Fonoaudiología, Universidad San Sebastián, Santiago de Chile, Chile. [9]Grupo de Bioingeniería, Decanato de Investigación, Universidad Nacional Experimental del Táchira, San Cristóbal, Venezuela. [10]Advanced Center for Electrical and Electronic Engineering, Universidad Técnica Federico Santa María, Valparaíso, Chile. [11]University of Buenos Aires, Buenos Aires, Argentina. [12]The Clinical Hospital of Chengdu Brain Sciences Institute, University of Electronic Sciences and Technology of China, Chengdu, China. [13]Technology of China, Chengdu, China. [14]Cuban Neuroscience Center, La Habana, Cuba. [15]Grupo de Neurociencias de Antioquia (GNA), University of Antioquia, Medellín, Colombia. [16]Department of Psychology, Master Program of Clinical Neuropsychology, Universidad Surcolombiana Neiva, Neiva, Colombia. [17]Department of Psychology, Universidad Cooperativa de Colombia, Arauca, Colombia. [18]Neurocognition and Psychophysiology Laboratory, Universidad Surcolombiana, Neiva, Colombia. [19]Reference Center of Behavioural Disturbances and Dementia, School of Medicine, University of Sao Paulo, Sao Paulo, Brazil. [20]Traumatic Brain Injury Cognitive Rehabilitation Out-Patient Center, University of Sao Paulo, Sao Paulo, Brazil. [21]Center for Social and Cognitive Neuroscience, School of Psychology, Universidad Adolfo Ibáñez, Santiago, Chile. [22]Neuropsychology and Clinical Neuroscience Laboratory (LANNEC), Physiopathology Program-Institute of Biomedical Sciences (ICBM), Neuroscience and East Neuroscience Departments, University of Chile, Santiago, Chile. [23]Centro de Neuropsicología Clínica (CNC), Santiago, Chile. [24]Faculty of Medicine, Izmir University of Economics, Izmir, Turkey. [25]Brain Dynamics Multidisciplinary Research Center, Dokuz Eylul University, Izmir, Turkey. [26]Izmir Biomedicine and Genome Center, Izmir, Turkey. [27]School of Engineering, Institute for Imaging, Data and Communications, University of Edinburgh, Edinburgh, UK. [28]Department of Physiology and Pharmacology 'V. Erspamer', Sapienza University of Rome, Rome, Italy. [29]Hospital San Raffaele Cassino, Cassino, Italy. [30]School of Psychology, Trinity College Dublin, Dublin, Ireland. [31]Department of Neurosciences, Health Sciences Institute, Istanbul Medipol University, İstanbul, Turkey. [32]Health Sciences and Technology Research Institute (SABITA), Istanbul Medipol University, Istanbul, Turkey. [33]Department of Biophysics, School of Medicine, Istanbul Medipol University, Istanbul, Turkey. [34]Pontificia Universidad Javeriana (PhD Program in Neuroscience), Bogotá, Colombia. [35]Center of Memory and Cognition Intellectus, Hospital Universitario San Ignacio Bogotá, San Ignacio, Colombia. [36]Departamento de Medicina Legal, Psiquiatría y Patología, Universidad Complutense de Madrid, Madrid, Spain. [37]Department of Electronic and Electrical Engineering, University of Strathclyde, Glasgow, UK. [38]Universidad Católica San Pablo, Arequipa, Peru. [39]Centro Interdisciplinario de Neurociencia de Valparaíso (CINV), Universidad de Valparaíso, Valparaíso, Chile. [40]Departamento de Estudios Psicológicos, Universidad ICESI, Cali, Colombia. [41]Centre for Biomedical Engineering, School of Mechanical Engineering Sciences, University of Surrey, Guildford, UK. [42]School of Psychology, University of Glasgow, Glasgow, UK. [43]Institute for Complex Systems and Mathematical Biology, University of Aberdeen, Aberdeen, UK. [44]Centre for Signal and Image Processing, Department of Electronic and Electrical Engineering, University of Strathclyde, Strathclyde, UK. [45]Sorbonne Université, Institut du Cerveau - Paris Brain Institute - ICM, InsermCNRS, Paris, France. [46]Department of Neurosciences, Health Sciences Institute, Dokuz Eylül University, Izmir, Turkey. [47]Harvard Medical School, Boston, MA, USA. [48]Department of Psychological Sciences and Health, University of Strathclyde, Glasgow, UK. [49]BrainLat, Universidad Adolfo Ibáñez, Santiago, Chile. [50]Departamento de Lingüística y Literatura, Universidad de Santiago de Chile, Santiago, Chile. [51]Mental Health Department, Hospital Universitario Fundación Santa Fe, Bogota, Colombia. [52]Department of Geriatrics, Instituto Nacional de Ciencias Médicas y Nutrición Salvador Zubirán, Mexico City, Mexico. [53]Memory and Neuropsychiatric Center (CMYN), Neurology Department, Hospital del Salvador and Faculty of Medicine, University of Chile, Santiago, Chile. [54]Geroscience Center for Brain Health and Metabolism (GERO), Santiago, Chile. [55]Neuropsychology and Clinical Neuroscience Laboratory (LANNEC), Physiopathology Program – Institute of Biomedical Sciences (ICBM), Neuroscience and East Neuroscience Departments, University of Chile, Santiago, Chile. [56]Neurology and Psychiatry Department, Clínica Alemana-Universidad Desarrollo, Santiago, Chile. [57]Centro de Investigación Clínica Avanzada (CICA), Universidad de Chile, Santiago, Chile. [58]Departamento de Neurología y Neurocirugía, Hospital Clínico de la Universidad de Chile, Santiago, Chile. [59]Departamento de Neurociencia, Universidad de Chile, Santiago, Chile. [60]Servicio de Neurología, Instituto Peruano de Neurociencias, Lima, Perú. [61]Facultad de Psicología, Universidad del Valle, Cali, Colombia. [62]Cognitive Science Group, Instituto de Investigaciones Psicológicas (IIPsi), CONICET UNC, Universidad Nacional de Córdoba, Córdoba, Argentina. [63]Centro de Neuropsiquiatría y Neurología de la Conducta (CENECON), Universidad de Buenos Aires (UBA), Buenos Aires, Argentina. [64]Instituto de Ciencias Biomédicas (ICBM), Universidad Catoóica de Cuyo, San Juan, Argentina. [65]Instituto Nacional de Neurologia y Neurocirugia MVS, Universidad Nacional Autonoma de Mexico, Mexico City, Mexico. [66]Memory and Aging Center, Department of Neurology, Weill Institute for Neurosciences, University of California, San Francisco, CA, USA. [67]Cognitive and Behavioral Neurology Unit, Hospital das Clinicas, University of São Paulo Medical School, São Paulo, Brazil. [68]Universidade Federal de Minas Gerais, Belo Horizonte, Brazil. [69]School of Engineering, Department of Electrical and Electronic Engineering, Trinity College Dublin, Dublin, Ireland. [70]Trinity College Institute of Neuroscience, Trinity College Dublin, Dublin, Ireland. [71]Trinity Centre for Biomedical Engineering, Trinity College Dublin, Dublin, Ireland. [72]Division of the Biological Sciences, The University of Chicago, Chicago, IL, USA. [73]These authors contributed equally: Sebastian Moguilner, Sandra Baez. ✉e-mail: agustin.ibanez@gbhi.org

Methods

The total dataset consisted of 5,306 participants, with 2,953 undergoing fMRI and 2,353 EEG acquisitions. Of these, 3,509 were controls, 517 had MCI, 828 had Alzheimer disease and 463 had bvFTD.

fMRI dataset

The fMRI dataset involved 2,953 participants from both non-LAC (USA, China, Japan) and LAC (Argentina, Chile, Colombia, Mexico, Peru), including 1,444 healthy controls. Two hundred and fifteen participants met the Petersen criteria for MCI with a 24 Mini-Mental State Examination (MMSE) cut-off value, 719 were diagnosed as probable Alzheimer disease[61], and 402 fulfilled the diagnostic criteria for bvFTD[62]. LAC participants were recruited from the Multi-Partner Consortium to Expand Dementia Research in Latin America (ReDLat, with participants from Mexico, Colombia, Peru, Chile and Argentina)[63]. Non-LAC participants were non-Latino individuals from ReDLat, the Alzheimer's Disease Neuroimaging Initiative and the Neuroimaging in Frontotemporal Dementia repository. The datasets were matched on sex, age and years of education (Table 1). Sex information was determined by self-report. No information regarding gender was inquired. To ensure data reliability, we excluded subjects who reported a history of alcohol/drug abuse or psychiatric or other neurological illnesses.

EEG dataset

The total dataset involved 2,353 participants. Controls comprised 1,183 participants, including 737 from non-LAC (Turkey, Greece, Italy, UK and Ireland) and 446 from LAC (Cuba, Colombia, Brazil, Argentina and Chile). Participants presenting with clinical conditions were recruited from a multisite study with harmonized assessments[25,36,63] in LAC (Argentina, Brazil, Chile and Colombia). This dataset included 133 patients with MCI, 108 with Alzheimer disease, and 57 with bvFTD. The controls datasets were matched on age, sex and years of education concerning the clinical groups (MCI, Alzheimer disease and bvFTD) (Table 1). Sex information was determined by self-report. No information regarding gender was inquired. The diagnostic criteria for MCI, Alzheimer disease and bvFTD were the same as those used for the fMRI dataset. No subject in any of the clinical conditions reported a history of alcohol/drug abuse, psychiatric, or other neurological illnesses.

Ethics approval

The local institutions that contributed EEGs and/or fMRIs to this study approved the acquisitions and protocols (Supplementary Data 1), and all participants signed a consent form following the declaration of Helsinki. The overall study was approved by the consortium under multiple institutional review boards (FWA00028264, FWA00001035, FWA00028864, FWA00001113, FWA00010121, FWAA00014416, FWA00008475, FWA00029236, FWA00029089 and FWA00000068). Data collection and analysis posed no risks concerning stigmatization, incrimination, discrimination, animal welfare, environmental, health, safety, security or personal concerns. No transfer of biological materials, cultural artifacts or traditional knowledge occurred. The authors reviewed pertinent studies from all countries while preparing the manuscript.

fMRI preprocessing

The images were obtained from different scanners and in distinct acquisition settings (Supplementary Table 4). We included closed and open eyes recordings to increase the sample size for resting-state fMRI (rs-fMRI) data. The type of resting-state recording was controlled by a dummy variable (open or closed eyes) when using the functional connectivity metric[64]. The resting state of fMRI preprocessing was conducted using the fmriprep toolbox (v.22.0.2). Additional preprocessing was performed using the CONN22 (ref. 64) toolbox and including smoothing with a Gaussian kernel of 6 × 6 × 6 mm, the signal denoising through linear regression to account for confounding effects of white matter, cerebrospinal fluid, realignment, and scrubbing. A band-pass filter (0.008–0.09 Hz) was applied. After time series preprocessing, we used region-of-interest analysis based on the brain regions of the Automated Anatomical Labeling (AAL90) atlas to reduce the dimensionality of the fMRI data for machine learning algorithms.

EEG preprocessing

EEGs were processed offline using procedures implemented in a custom, automatic pipeline for computing brain functional connectivity using a mesh model for multiple electrode arrays and source space estimation (see Supplementary Table 5 for acquisition parameters). The pipeline allows for the multicentric assessment of resting-state EEG (rsEEG) connectivity and has been validated in a large-scale evaluation of connectivity in dementia[65]. Recordings were re-referenced to the average reference and band-pass filtered between 0.5 and 40 Hz using a zero-phase shift Butterworth filter of order 8. Data were downsampled to 512 Hz, referenced using the reference electrode standardization technique, and corrected for cardiac, ocular and muscular artifacts using two methods based on independent component analysis. ICLabel (a tool for classifying EEG independent components into signals and different noise categories)[66], and EyeCatch (a tool for identifying eye-related independent component analysis scalp maps) were used[67]. Data were visually inspected after artifact correction, and malfunctioning channels were identified and replaced using weighted spherical interpolations.

EEG normalization. Following guidelines for multicentric studies[37], EEG was rescaled to reduce cross-site variability. The normalization was carried out separately for each dataset and consisted of the *Z*-score transformation of the EEG time series. The *Z*-score quantifies the distance of raw data from the mean in standard deviation units. The *Z*-score transformed EEG connectivity matrices display more prominent interhemispheric asymmetry and reinforced long-distance connections than unweighted connectivity representations[65].

EEG source space estimation. The source analysis of the rsEEG was conducted using the standardized low-resolution electromagnetic tomography method (sLORETA). sLORETA allows estimating the standardized current density at each of the predefined virtual sensors located in the cortical gray matter and the hippocampus of a reference brain (MNI 305, Brain Imaging Centre, Montreal Neurologic Institute) based on the linear, weighted sum of a particular scalp voltage distribution or the EEG cross-spectrum at the sensor level. sLORETA is a distributed EEG inverse solution method based on an appropriate standardized version of the minimum norm current density estimation. sLORETA overcomes problems intrinsic to the estimation of deep sources of EEG and provides exact localization to test seeds, albeit with a high correlation between neighboring generators.

The different electrode layouts were registered onto the scalp MNI 152 coordinates. A signal-to-noise ratio of 1 was chosen for the regularization method used to compute the sLORETA transformation matrix (forward operator for the inverse solution problem). The standardized current density maps were obtained using a head model of three concentric spheres in a predefined source space of 6,242 voxels (voxel size = 5 mm^3) of the MNI average brain. A brain segmentation of 82 anatomic compartments (subcortical and cortical areas) was implemented using the automated anatomical labeling (AAL90) atlas. Current densities were estimated for the 153,600 voltage distributions comprising the 5 min of rsEEG (sampled at 512 Hz). The voxels belonging to the same AAL region were averaged such that a single (mean) time series was obtained for each cortical region[32,68,69].

High-order interactions

After preprocessing 82 time series from the AAL brain parcellation for fMRI and EEG, we calculated the high-order interactions across triplets

composed of a region i and region j and a set comprising all the brain regions without i and j. We evaluated high-order interactions using the organizational information (Ω) metric, a multivariate extension of Shannon's mutual information, which assesses the dominant characteristic of multivariate systems (high-order interactions). To operationalize the Shannon entropy, we used the Gaussian copula approximation, which estimates the differential Shannon's entropy from the covariance matrix of the Gaussian copula transformed data[70]. This is a mixture of a parametric and a nonparametric approach, as the copula is preserved in a nonparametric way but is then used to generate Gaussian marginals. The Ω quantifies the balance between redundancy and synergy in high-order interactions among brain regions. By definition, $\Omega > 0$ implies that the interdependencies are better described as shared randomness, indicating redundancy dominance. Conversely, $\Omega < 0$ suggests that the interdependencies are better explained as collective constraints, indicating synergy dominance. After normalization, its magnitude ranges from −1 to 1. Ω can be expressed as:

$$\Omega(\mathbf{X}^n) = (n-2)H(\mathbf{X}^n) + \sum_{j=1}^{n}\left[H(X_j) - H(\mathbf{X}^n_{-j})\right] \quad (1)$$

where $\mathbf{X}^n$ is the random vector that describes the system and H is the Shannon's entropy. When n is reduced to three variables (x, y and z), Ω can be expressed as

$$\Omega(x,y,z) = H(x,y,z) - H(x,y) - H(x,z) - H(y,z) + H(x) + H(y) + H(z) \quad (2)$$

To analyze brain activity, z can be considered a multivariate time series representing the activity of all brain regions except for x and y. Therefore, O-info measures how synergistic or redundant is the relationship between two brain regions concerning the rest of the regions.

Model input preprocessing

As input to the models, the weighted adjacency matrix corresponding to the Ω metric was converted to a graph. This matrix defines the edges in the graph, where the weight of each edge reflects the Ω value between the corresponding regions. The feature vectors at each graph node are derived from the O-info matrix; specifically, each node's feature vector is the corresponding row in the Ω matrix. To this end, the connectivity matrices were first converted to tensors using the PyTorch deep learning library v.2.3.0, enabling their efficient manipulation. These tensors were reshaped, organizing the connectivity data into a structure where each tensor represented the features of nodes within a graph. This transformation preserved the relational information from the original matrices, making it accessible for analysis by graph neural networks. To ensure the integrity of the data, graphs containing not a number (NaN) values, either in their features or target values, were filtered out. The remaining graphs were then split into training and validation sets using a stratified split to ensure a balanced representation of age groups in both sets.

Data augmentation

We used augmentation tailored for connectivity matrices to make the model more resilient to heterogeneity and generalizability. Linear interpolation between matrices corresponding to neighboring age values was used, in contrast to traditional image augmentation techniques such as random rotations or crops that are inappropriate for connectivity data.

Given two matrices, M_1 and M_2, representing fMRI or EEG connectivity at ages a_1 and a_2, respectively, the interpolation to produce a matrix for a target age where $a_1 < a_t < a_2$ was conducted using the formula:

$$M_t = (1-\alpha)M_1 + \alpha M_2 \quad (3)$$

Here, $\alpha = \frac{a_t - a_1}{a_2 - a_1}$ represents the interpolation factor.

This augmentation method enabled the generation of fMRI and EEG connectivity matrices for age values previously absent in the data set. The derived matrices, through interpolation, ensure a smooth transition in the fMRI and EEG patterns from one age value to another, thereby maintaining the inherent physiological significance of the original data—preliminary validation against a hold-out dataset showed improvements in model fit against dataset heterogeneity. We included 500 samples with data augmentation only the training datasets for both modalities, half for the non-LAC and half for the LAC samples.

The architecture of the models

Two GCNs[71] were designed, tailored to process graph-structured data. We used the PyTorch Geometric code library v.2.5.3 based on the PyTorch library v.2.3.0 to develop and train the models. Two models were created, one for fMRI data and another for EEG data. Unlike traditional convolutional networks suited for neuroimaging data, functional connectivity demands a specialized approach because neighboring data points are not necessarily close in native space (adjacent brain areas). The GCN uses adjacency matrices of graphs as inputs comprised of node features. Each node in the graph aggregates features from its neighbors through a series of operations, including multiplication by a normalized adjacency matrix, transformation using a weight matrix, and applying an activation function, here the ReLU[72]. The architecture consisted of two graph convolutional layers. The input features (O-info matrix) were passed through the first convolutional layer, followed by a ReLU activation function and a dropout layer for regularization. The features were then passed through the second convolutional layer. Finally, average pooling was used to aggregate the output features. To train the two models, we combined mean squared error as the loss function and the Adam optimizer. Given the variability in the data and potential model configurations, we implemented a hyperparameter tuning process using a grid search over specified learning rates and epoch numbers. For each model for the controls, the data was initially split into 80% for training and validation, and 20% for hold-out testing. Within the 80% training and validation set, we applied fivefold cross-validation to determine the optimal hyperparameters for the model. After determining the best hyperparameters through this cross-validation process, the final model's performance was evaluated on the remaining 20% hold-out test set to assess its generalization capability[73].

Statistical analyses

Following hyperparameter tuning, each model was retrained using the best hyperparameters on the training set and evaluated on the test set. For a more comprehensive assessment, the predicted age values were compared with the actual age values using Pearson's correlation coefficient, R^2 and Cohen's f^2 effect size for each model[74]. We used the method outlined below to evaluate if the model was predicting increased or decreased ages concerning the actual chronological age. All statistical analyses were run using Python v.3.9.13.

The MDE is a diagnostic metric used to evaluate the prediction accuracy of the models, specifically focusing on the direction of prediction gaps rather than their magnitude to detect bias. It is calculated as follows:

$$\mathrm{MDE} = \frac{1}{n}\sum_{i=1}^{n}(y_i - \hat{y}_i) \quad (4)$$

The function 'sign' yields a value of +1 if the prediction is above the actual value, −1 if below, and 0 if they are equal. y_i is the real age of subject i and $\hat{y}_i$ is the predicted age. An MDE value close to zero suggests a balanced number of overestimations and underestimations. Positive or negative values indicate systematic biases in the prediction method, where a positive MDE means the model generally overpredicts, and a negative MDE indicates underprediction.

We examined potential regional biases in predictive accuracy and possible sex effects or signal acquisition noise. The statistical approach involved conducting permutation tests (5,000 subsample iterations each), a nonparametric statistical test that does not assume a specific distribution of the data. Given the nature of the permutation test, our analysis constituted two-sided tests, assessing the likelihood of observing the obtained difference under the null hypothesis of no difference between the models. Although the permutation test alleviates the need for normality assumptions, making it resilient to deviations from normal distribution, it addresses multiple comparison concerns by evaluating the empirical distribution of the test statistic under the null hypothesis.

We compared the adequacy of the models using the r.m.s.e. This is a metric to quantify the discrepancies between predicted and observed values in modeling, given by the formula:

$$\text{r.m.s.e.} = \sqrt{\frac{1}{N}\sum_{i=1}^{n}(y_i - \hat{y}_i)^2} \quad (5)$$

In this equation, y_i is the observed value, $\hat{y_i}$ is the predicted value and N is the total number of observations. The r.m.s.e. measures the average magnitude of errors between predicted and actual observations. The squaring process results in a higher weight to outliers, making it a useful measure to evaluate if a model is robust to outliers.

To evaluate feature importance, we used bootstrapping to assess the significance of individual nodes (brain areas) and edges (connections between brain nodes/regions) within the graph neural network. With this approach, we executed a two-step process to quantify the node and its edge's impact on the model's predictions. Initially, the model's output was calculated with all nodes and its edges present to establish a baseline performance metric. Subsequently, the analysis was repeated after removing each node and edge at a time, thus simulating network information absence. The difference in the model's output, with and without each area and edge was quantified, providing a measure of the network node importance. This process was repeated across multiple bootstrap testing dataset samples (n = 5,000) to calculate confidence intervals (CI). Finally, a feature importance list of nodes was generated in descending order of importance for brain-age prediction. This methodological framework allowed for an analysis of network-level contributions to each model's overall predictive performance.

Gradient-boosting regression models. We used gradient-boosting regression models[75] to investigate the impact of factors associated with the physical and social exposomes, and disease disparities, on brain-age gaps between LAC and non-LAC populations. As predictors, we included country-level measures of: (1) air pollution (PM2.5 exposure); (2) socioeconomic inequality (the Gini index)[76]; (3) the burden of communicable, maternal, prenatal and nutritional conditions; and (4) the burden of noncommunicable diseases. These indicators were sourced from the updated country-specific data provided on the World Bank's platform (https://databank.worldbank.org/). In addition, individual neurocognitive status (being controls versus having Alzheimer disease, MCI or bvFTD) was included as predictor. Brain-age gaps from fMRI and EEG datasets were the outcomes.

Models were trained using 90% of the dataset and subsequently tested on an independent 10% subset, using a 10-fold cross-validation framework. The cross-validation was repeated 10 times. Within each iteration, estimation coefficients for the predictors, as well as the R^2, Cohen's f^2 (ref. 74) and r.m.s.e., were computed. We assessed feature importance using a multi-method approach incorporating permutation importance, features importance based on the MDI and SHAP values[77]. We provided the mean importance values for each method, along with their 99% CI, as well as the average R^2 and Cohen's f^2 (ref. 74). Features whose lower confidence interval boundary crosses zero are considered nonsignificant. To optimize Ridge's hyperparameters, Bayesian optimization was used.

Following the same multi-method approach, we conducted gradient-boosting regressions to explore the effect of gender inequality and sex on brain-age gaps. As predictors, we included: (1) the country-level GII, a composite metric measuring reproductive health, empowerment and the labor market; (2) sex; (3) region (LAC versus non-LAC); and (4) individual neurocognitive status (healthy controls versus Alzheimer disease, MCI or bvFTD). Brain-age gaps from fMRI and EEG were the outcomes.

Data quality assessment. For the fMRI overall data quality (ODQ) metric, each time series was segmented in 20 repetition time (TR) length to evaluate the temporal signal-to-noise ratio (tSNR)[78], which is calculated as the mean fMRI signal divided by its standard deviation within each segment. Segments with tSNR above a threshold of 50 were classified as high quality[78]. As additional evaluations, we checked the variability of the tSNR segments of all the time series in the brain to check for spatial consistency. Lastly, we checked for remaining outliers as signal spikes from movement or transient gradient artifacts. Thus, the fMRI ODQ was computed as a percentage of good segments considering its tSNR, low spatial variability and the number of segments not having spikes from movement or transient gradient remaining artifacts.

For the EEG data quality assessment[79], signals were divided into 1-s segments, and the quality of each segment was evaluated using four specific metrics. These metrics included the detection of weak or constant signals based on standard deviation, the identification of artifacts through signal amplitude ratios, the presence of high-frequency noise and low correlation between channels. The EEG ODQ was then calculated as the percentage of segments exhibiting good quality. A value of 0 indicated that all segments were of poor quality, whereas a value of 100 indicated that all segments were of high quality.

Sensitivity analyses. We examined whether variations in fMRI or EEG data quality explained the differences in brain age between the non-LAC and LAC, comparing different groups' fMRI[78] and EEG[79] data quality metrics, with subsample permutation tests with 5,000 iterations for each comparison. In addition, we conducted a linear regression to examine the association between the fMRI data quality metrics and the brain-age gaps. To further control for scanner effects, we implemented an additional harmonization strategy in the fMRI training dataset. This method involves normalizing the brain-age gap variable within each scanner type by scaling the data to a fixed range using the min–max scaler[14]. This ensures that the minimum and maximum values of the brain-age gap variable are consistent across different scanners, thereby reducing variability caused by scanner differences. In addition, we accounted for the sign of the brain-age gap after normalization to maintain the interpretability of positive and negative values. This procedure adjusts for location and scale differences (for example, mean and variance) across sites, minimizing scanner-related variability.

We used permutation tests (5,000 subsample iterations each) to compare the brain-age gaps between subsamples of participants undergoing fMRI with open versus closed eyes. We included 124 controls with closed eyes and 86 with open eyes, 269 Alzheimer disease with closed eyes and 164 with open eyes, and 88 bvFTD with closed eyes and 69 with open eyes. Notably, all MCI participants underwent fMRI with open eyes. Our findings revealed no significant differences in brain-age gaps when analyzing data from open versus closed eyes conditions across all group comparisons (permutation test = 5,000 iterations).

Ethics and inclusion statement

This work involved a collaboration between researchers in multiple countries. Contributors from different sites are included as coauthors according to their contributions. Researchers residing in low and middle income countries (LMIC) were involved in study design, study

implementation, methodological procedure, writing and reviewing processes. The current research is locally relevant due to the larger disparities observed in LAC and other regions. Roles and responsibilities were agreed among collaborators ahead of the research. Ethics committees approved all research involving participants. To prevent any stigmatization, all identifying information has been removed to preserve the privacy of individuals. We endorse the Nature Portfolio journals' guidance on LMIC authorship and inclusion. Authorship was based on the intellectual contribution, commitment, and involvement of each researcher in this study. We included authors born in LMICs and other underrepresented countries.

Reporting summary

Further information on research design is available in the Nature Portfolio Reporting Summary linked to this article.

Data availability

All preprocessed data are openly available at: https://osf.io/8zjf4/. The fMRI and EEG datasets comprise sources: (1) currently publicly available for direct download after registration and access application, (2) available after contacting the researcher or (3) accessible after IRB approval of formal data-sharing agreement in a process that can last up to 12 weeks. The fMRI sources that are publicly available for direct download are the following: Alzheimer's Disease Neuroimaging Initiative (ADNI) (USA) (https://ida.loni.usc.edu/collaboration/access/appLicense.jsp), Chinese Human Connectome Project (CHCP) (China) (https://scidb.cn/en/detail?dataSetId=f512d085f3d3452a9b14689e9997ca94#p2), The Frontotemporal Lobar Degeneration Neuroimaging Initiative (FTLDNI) (USA) (https://ida.loni.usc.edu/collaboration/access/appLicense.jsp) and the Japanese Strategic Research Program for the Promotion of Brain Science (SRPBS) (Japan) (https://bicr-resource.atr.jp/srpbsopen/). The fMRI sources available after contacting the researcher include ReDLat USA by contacting Bruce Miller at UCSF through datasharing@ucsf.edu. The fMRI sources that require IRB approval and a formal data-sharing agreement include: ReDLat pros (Argentina, Chile, Colombia, Mexico, Peru) by contacting Agustín Ibañez at agustin.ibanez@gbhi.org, Centro de Gerociencia Salud Mental y Metabolismo (GERO) (Chile) by contacting Andrea Slachevsky at andrea.slachevsky@uchile.cl, ReDLat pre (Argentina) by contacting Agustín Ibañez at agustin.ibanez@gbhi.org, ReDLat pre (Peru) by contacting Nilton Custodio at ncustodio@ipn.pe, ReDLat pre (Colombia) by contacting Diana Matallana at dianamat@javeriana.edu.co, ReDLat pre (Colombia-II) by contacting Felipe Cardona at felipe.cardona@correounivalle.edu.co, ReDLat pre (Mexico) by contacting Ana Luisa Sosa at drasosa@hotmail.com, ReDLat pre (Chile) by contacting María Isabel Behrens at behrensl@uchile.cl and ReDLat pre (Chile) by contacting Andrea Slachevsky at andrea.slachevsky@uchile.cl. The EEG sources that are publicly available for direct download are Centro de Neurociencias de Cuba (CHBMP) (Cuba) (https://www.synapse.org/Synapse:syn22324937). The EEG sources that are available after contacting the researcher include BrainLat (Argentina) by contacting Agustina Legaz at alegaz@udesa.edu.ar, BrainLat (Chile) by contacting Agustina Legaz at alegaz@udesa.edu.ar, Izmir University of Economics (Turkey) by contacting Gorsev Gener at gorsev.yener@ieu.edu.tr, Trinity College Dublin (Ireland) by contacting Francesca Farina at francesca.farina@northwestern.edu, Universidad de Antioquia (Colombia) by contacting Francisco Lopera at floperar@gmail.com, Universidad de Sao Paulo (Brazil) by contacting Mario Parra at mario.parra-rodriguez@strath.ac.uk, Universidad de Roma La Sapienza (Italy) by contacting Susana Lopez at susanna.lopez@uniroma1.it, University of Strathclyde (UK) by contacting Mario Parra at mario.parra-rodriguez@strath.ac.uk, Istanbul Medipol University (Turkey) by contacting Tuba Aktürk at takturk@medipol.edu.tr and Takeda (Chile) by contacting Daniela Olivares at danielaolivaresvargas@gmail.com. Indicators of air pollution, socioeconomic inequality (the Gini index), the burden of communicable, maternal, prenatal and nutritional conditions, and the burden of noncommunicable diseases were sourced from the updated country-specific data provided on the World Bank's platform (https://databank.worldbank.org/). Country-level GII are available on the World Health Organization's website (https://www.who.int/data/nutrition/nlis/info/gender-inequality-index-(gii)). For additional details, see Supplementary Data 1.

Code availability

The code used to preprocess and analyze the data of this work is available in an Open Science Foundation repository at the following address: https://osf.io/8zjf4/.

References

61. McKhann, G. M. et al. The diagnosis of dementia due to Alzheimer's disease: recommendations from the National Institute on Aging-Alzheimer's Association workgroups on diagnostic guidelines for Alzheimer's disease. *Alzheimers Dement.* **7**, 263–269 (2011).
62. Rascovsky, K. et al. Sensitivity of revised diagnostic criteria for the behavioural variant of frontotemporal dementia. *Brain* **134**, 2456–2477 (2011).
63. Prado, P. et al. The BrainLat project, a multimodal neuroimaging dataset of neurodegeneration from underrepresented backgrounds. *Sci. Data* **10**, 889 (2023).
64. Nieto-Castanon, A. *Handbook of Functional Connectivity Magnetic Resonance Imaging Methods in CONN* 108 (Hilbert, 2020).
65. Prado, P. et al. Harmonized multi-metric and multi-centric assessment of EEG source space connectivity for dementia characterization. *Alzheimers Dement. (Amst.)* **15**, e12455 (2023).
66. Pion-Tonachini, L., Kreutz-Delgado, K. & Makeig, S. ICLabel: an automated electroencephalographic independent component classifier, dataset, and website. *Neuroimage* **198**, 181–197 (2019).
67. Bigdely-Shamlo, N., Kreutz-Delgado, K., Kothe, C. & Makeig, S. EyeCatch: data-mining over half a million EEG independent components to construct a fully-automated eye-component detector. *Annu. Int. Conf. IEEE Eng. Med. Biol. Soc.* **2013**, 5845–5848 (2013).
68. Cruzat, J. et al. Temporal irreversibility of large-scale brain dynamics in Alzheimer's disease. *J. Neurosci.* **43**, 1643–1656 (2023).
69. Prado, P. et al. Source space connectomics of neurodegeneration: one-metric approach does not fit all. *Neurobiol. Dis.* **179**, 106047 (2023).
70. Ince, R. A. et al. A statistical framework for neuroimaging data analysis based on mutual information estimated via a gaussian copula. *Hum. Brain Mapp.* **38**, 1541–1573 (2017).
71. Li, Y. et al. Brain connectivity based graph convolutional networks and its application to infant age prediction. *IEEE Trans. Med. Imaging* **41**, 2764–2776 (2022).
72. Zhou, Y., Huo, H., Hou, Z. & Bu, F. A deep graph convolutional neural network architecture for graph classification. *PLoS ONE* **18**, e0279604 (2023).
73. Kohavi, R. A study of cross-validation and bootstrap for accuracy estimation and model selection. *Proc. of 14th International Joint Conference on AI* 1137–1143 (1995).
74. Selya, A. S., Rose, J. S., Dierker, L. C., Hedeker, D. & Mermelstein, R. J. A practical guide to calculating Cohen's f(2), a measure of local effect size, from PROC MIXED. *Front. Psychol.* **3**, 111 (2012).
75. Friedman, J. Greedy function approximation: a gradient boosting machine. *Ann. Statist.* **29**, 1189–1232 (2001).
76. Gini, C. *Variabilità e mutabilità: contributo allo studio delle distribuzioni e delle relazioni statistiche [Fasc. I.]*. (Tipogr. di P. Cuppini, 1912).

77. Chen, H., Lundberg, S. M. & Lee, S.-I. Explaining a series of models by propagating Shapley values. *Nat. Commun.* **13**, 4512 (2022).
78. Murphy, K., Bodurka, J. & Bandettini, P. A. How long to scan? The relationship between fMRI temporal signal to noise ratio and necessary scan duration. *Neuroimage* **34**, 565–574 (2007).
79. Zhao, L. et al. Quantitative signal quality assessment for large-scale continuous scalp electroencephalography from a big data perspective. *Physiol. Meas.* **44**, 035009 (2023).

Acknowledgements

This work was supported by Latin American Brain Health Institute (BrainLat) grant no. BL-SRGP2020-02 awarded to M.A.P. and A.I. A.I. is supported by grants from ReDLat (National Institutes of Health and the Fogarty International Center, National Institutes of Aging (grant nos. R01 AG057234, R01 AG075775, R01 AG021051, R01 AG083799, CARDS-NIH 75N95022C00031), Alzheimer's Association (grant no. SG-20-725707), Rainwater Charitable Foundation, The Bluefield project to cure frontotemporal dementia and Global Brain Health Institute)), ANID/FONDECYT Regular (grant nos. 1210195, 1210176 and 1220995) and ANID/FONDAP/15150012. A.M.G. is partially supported by the National Institute on Aging of the National Institutes of Health (grant nos. R01AG075775, R01AG083799, 2P01AG019724), ANID (FONDECYT Regular grant nos. 1210176 and 1210195) and DICYT-USACH (grant no. 032351G_DAS). The contents of this publication are solely the author's responsibility and do not represent the official views of these institutions. The funders had no role in study design, data collection and analysis, decision to publish or preparation of the manuscript.

Author contributions

A.I., S.M. and S.B. conceived the study. A.I. supervised the work. S.M. and H.H. were responsible for the study methodology and performed the analyses. R.G.-G., J. Cuadro, P.P. and A.L. collated the data. S.M., S.B. and A.I. interpreted the data. A.I., S.M. and S.B. wrote the original draft of the manuscript. All authors reviewed, edited, provided critical comments and approved the manuscript before submission.

Competing interests

The authors declare no competing interests.

Additional information

Extended data is available for this paper at https://doi.org/10.1038/s41591-024-03209-x.

Supplementary information The online version contains supplementary material available at https://doi.org/10.1038/s41591-024-03209-x.

Correspondence and requests for materials should be addressed to Agustin Ibanez.

Peer review information *Nature Medicine* thanks Wyllians Vendramini Borelli, B. T. Thomas Yeo and the other, anonymous, reviewer(s) for their contribution to the peer review of this work. Primary Handling Editor: Ming Yang, in collaboration with the *Nature Medicine* team.

https://doi.org/10.1038/s41591-024-03209-x

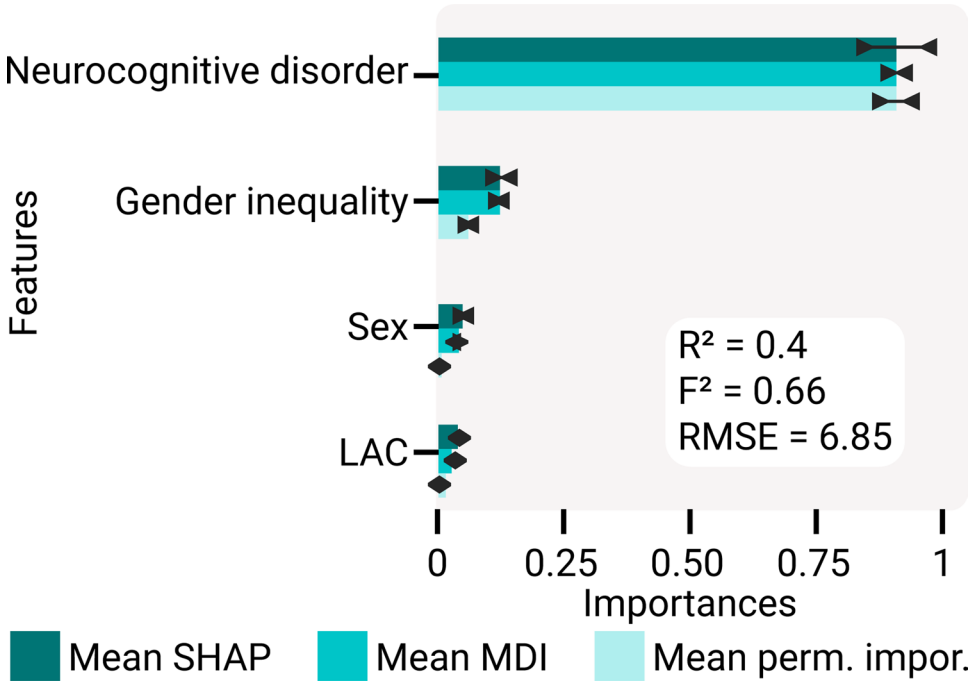

Extended Data Fig. 1 | Associations of sex and gender inequality with brain-age gaps. Multi-method approach comprising SHapley Additive exPlanations (SHAP) values, features and permutation importance. Plot shows the mean importance values for each method, along with their 99% confidence interval, as well as the average R-squared and Cohen's f^2. Having a neurocognitive disorder, being female, and living in countries with larger gender inequality (particularly from LAC), were associated with higher brain age-gaps. The model was significant with $R^2 = 0.40$ (99% CI ± 0.12), $F^2 = 0.66$ (99% CI ± 0.14), RMSE = 6.85 (99% CI ± 0.82), F = 352.54, and $p < 1e\text{-}15$. We conducted a two-sided F-test to evaluate the overall significance of the regression model. The importance of the features and their respective confidence intervals can be found in Supplementary Table 1. LAC = Latin American and Caribbean countries.

https://doi.org/10.1038/s41591-024-03209-x

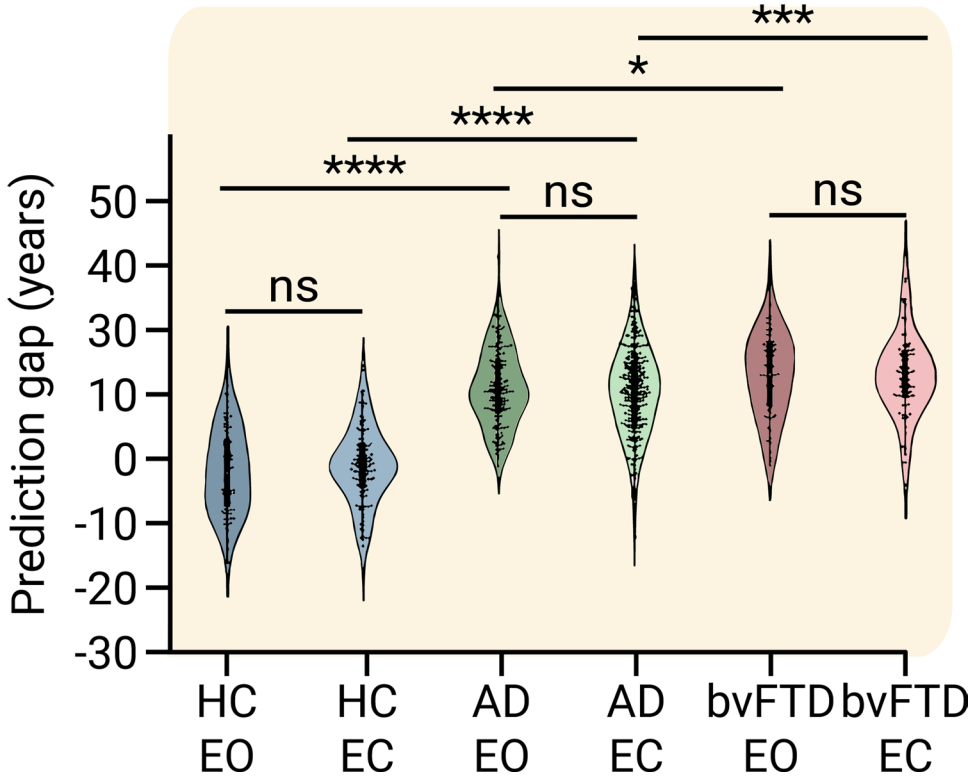

Extended Data Fig. 2 | Prediction gaps between fMRI datasets with either eyes open or eyes closed protocols. No significant differences were observed between participants with open vs. closed eyes within the same groups (two-sided permutation test, without multiple comparisons, and with 5000 algorithm iterations). We included 124 healthy controls with closed eyes and 86 with open eyes, 269 Alzheimer's disease participants with closed eyes and 164 with open eyes, and 88 behavioral variant frontotemporal dementia with closed eyes and 69 with open eyes. For HC eyes open vs AD eyes open $p < 1e\text{-}15$, for HC eyes closed vs AD eyes closed $p < 1e\text{-}15$, for AD eyes open vs bvFTD eyes open $p = 0.026$, for AD eyes closed vs bvFTD eyes closed $p = 0.004$. * $p < 0.05$, ** $p < 0.01$, *** $p < 0.001$. HC = healthy controls, AD = Alzheimer's disease, bvFTD = behavioral variant frontotemporal dementia, EC = eyes closed, EO = eyes open.

https://doi.org/10.1038/s41591-024-03209-x

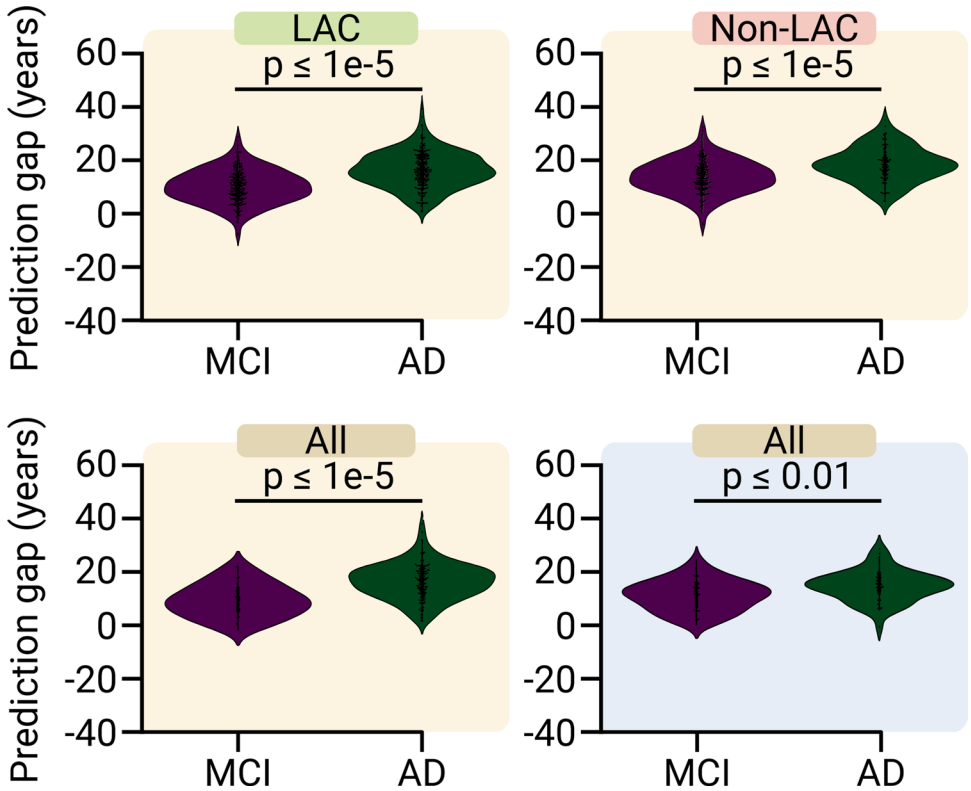

Extended Data Fig. 3 | Brain-age gaps between subsamples of mild cognitive impairment (MCI) and Alzheimer's disease (AD) groups matched by chronological age. Results were similar to those reported for the total MCI (n fMRI = 256, n EEG = 52) and AD (n fMRI = 254, n EEG = 52) datasets in Fig. 4a,b (two-sided permutation test, without multiple comparisons, and with 5000 algorithm iterations). For fMRI LAC $p < 1e\text{-}5$, for fMRI non-LAC $p < 1e\text{-}5$, for fMRI all $p < 1e\text{-}5$, for EEG all *p values* = 0.0024. fMRI LAC violin plots (Mean, q1, q3, whisker low, whisker high, minima, maxima): MCI = (10.550, 6.216, 14.748, −3.166, 26.203, −7.616, 29.185) and AD = (16.796, 12.591, 21.568, 1.133, 33.756, 1.133, 39.751). fMRI non-LAC: MCI = (10.518, 6.216, 14.565, −3.166, 26.203, −7.616, 29.185) and AD = (15.006, 11.076, 18.222, 1.133, 26.726, 1.133, 31.797). fMRI LAC: MCI = (10.702, 6.565, 15.222, −0.325, 23.516, −0.325, 23.516) and AD = (18.057, 13.681, 22.218, 2.916, 33.756, 2.916, 39.751). EEG all MCI = (11.813, 7.739, 15.804, 1.153, 24.775, 1.153, 24.775) and AD = (15.341, 12.727, 18.343, 6.751, 26.207, 0.348, 28.932). FMRI = functional magnetic imaging, EEG = electroencephalography, LAC = Latin American and Caribbean countries, HC = healthy controls, MCI = mild cognitive impairm)ent, AD = Alzheimer's disease, bvFTD = behavioral variant frontotemporal dementia.

nature portfolio

Corresponding author(s): Agustin Ibanez

Last updated by author(s): Jul 18, 2024

Reporting Summary

Nature Portfolio wishes to improve the reproducibility of the work that we publish. This form provides structure for consistency and transparency in reporting. For further information on Nature Portfolio policies, see our Editorial Policies and the Editorial Policy Checklist.

Statistics

For all statistical analyses, confirm that the following items are present in the figure legend, table legend, main text, or Methods section.

n/a	Confirmed	
☐	☒	The exact sample size (*n*) for each experimental group/condition, given as a discrete number and unit of measurement
☐	☒	A statement on whether measurements were taken from distinct samples or whether the same sample was measured repeatedly
☐	☒	The statistical test(s) used AND whether they are one- or two-sided *Only common tests should be described solely by name; describe more complex techniques in the Methods section.*
☐	☒	A description of all covariates tested
☐	☒	A description of any assumptions or corrections, such as tests of normality and adjustment for multiple comparisons
☐	☒	A full description of the statistical parameters including central tendency (e.g. means) or other basic estimates (e.g. regression coefficient) AND variation (e.g. standard deviation) or associated estimates of uncertainty (e.g. confidence intervals)
☐	☒	For null hypothesis testing, the test statistic (e.g. *F*, *t*, *r*) with confidence intervals, effect sizes, degrees of freedom and *P* value noted *Give P values as exact values whenever suitable.*
☒	☐	For Bayesian analysis, information on the choice of priors and Markov chain Monte Carlo settings
☒	☐	For hierarchical and complex designs, identification of the appropriate level for tests and full reporting of outcomes
☐	☒	Estimates of effect sizes (e.g. Cohen's *d*, Pearson's *r*), indicating how they were calculated

Our web collection on statistics for biologists contains articles on many of the points above.

Software and code

Policy information about availability of computer code

Data collection	No software was used for data collection
Data analysis	The code used to preprocess and analyze the data of this work is available in an Open Science Foundation repository at the following address: https://osf.io/8zjf4/

For manuscripts utilizing custom algorithms or software that are central to the research but not yet described in published literature, software must be made available to editors and reviewers. We strongly encourage code deposition in a community repository (e.g. GitHub). See the Nature Portfolio guidelines for submitting code & software for further information.

Data

Policy information about availability of data

All manuscripts must include a data availability statement. This statement should provide the following information, where applicable:

- Accession codes, unique identifiers, or web links for publicly available datasets
- A description of any restrictions on data availability
- For clinical datasets or third party data, please ensure that the statement adheres to our policy

All preprocessed data are openly available at: https://osf.io/8zjf4/. The fMRI and EEG datasets comprise sources (a) currently publicly available for direct download after registration and access application, (b) available after contacting the researcher, or (c) accessible after IRB approval of formal data-sharing agreement in a process that can last up to 12 weeks. The fMRI sources that are publicly available for direct download are the following: Alzheimer's Disease Neuroimaging Initiative

(ADNI) (USA) (ida.loni.usc.edu/collaboration/access/appLicense.jsp), Chinese Human Connectome Project (CHCP) (China) (scidb.cn/en/detail?dataSetId=f512d085f3d3452a9b14689e9997ca94#p2), The frontotemporal lobar degeneration neuroimaging initiative (FTLDNI) (USA) (ida.loni.usc.edu/collaboration/access/appLicense.jsp), and Japanese Strategic Research Program for the Promotion of Brain Science (SRPBS) (Japan) (bicr-resource.atr.jp/srpbsopen/). The fMRI sources available after contacting the researcher include ReDLat USA by contacting Bruce Miller at UCSF through datasharing@ucsf.edu. The fMRI sources that require IRB approval and a formal data sharing agreement include: ReDLat pros (Argentina, Chile, Colombia, Mexico, Peru) by contacting Agustín Ibañez at agustin.ibanez@gbhi.org, Centro de Gerociencia Salud Mental y Metabolismo (GERO) (Chile) by contacting Andrea Slachevsky at andrea.slachevsky@uchile.cl, ReDLat pre (Argentina) by contacting Agustín Ibañez at agustin.ibanez@gbhi.org, ReDLat pre (Peru) by contacting Nilton Custodio at ncustodio@ipn.pe, ReDLat pre (Colombia) by contacting Diana Matallana at dianamat@javeriana.edu.co, ReDLat pre (Colombia -II) by contacting Felipe Cardona at felipe.cardona@correounivalle.edu.co, ReDLat pre (Mexico) by contacting Ana Luisa Sosa at drasosa@hotmail.com, ReDLat pre (Chile) by contacting María Isabel Behrens at behrensl@uchile.cl, and ReDLat pre (Chile) by contacting Andrea Slachevsky at andrea.slachevsky@uchile.cl. The EEG sources that are publicly available for direct download are Centro de Neurociencias de Cuba (CHBMP) (Cuba) (www.synapse.org/Synapse:syn22324937). The EEG sources that are available after contacting the researcher include BrainLat (Argentina) by contacting Agustina Legaz at alegaz@udesa.edu.ar, BrainLat (Chile) by contacting Agustina Legaz at alegaz@udesa.edu.ar, Izmir University of Economics (Turkey) by contacting Gorsev Gener at gorsev.yener@ieu.edu.tr, Trinity College Dublin (Ireland) by contacting Francesca Farina at francesca.farina@northwestern.edu, Universidad de Antioquia (Colombia) by contacting Francisco Lopera at floperar@gmail.com, Universidad de Sao Paulo (Brazil) by contacting Mario Parra at mario.parra-rodriguez@strath.ac.uk, Universidad de Roma La Sapienza (Italy) by contacting Susana Lopez at susanna.lopez@uniroma1.it, University of Strathclyde (UK) by contacting Mario Parra at mario.parra-rodriguez@strath.ac.uk, Istanbul Medipol University (Turkey) by contacting Tuba Aktürk at takturk@medipol.edu.tr, and Takeda (Chile) by contacting Daniela Olivares at danielaolivaresvargas@gmail.com. Indicators of air pollution, socioeconomic inequality (the Gini index), the burden of communicable, maternal, prenatal, and nutritional conditions, and the burden of non-communicable diseases were sourced from the updated country-specific data provided on the World Bank's platform (https://databank.worldbank.org/). Country-level gender inequality indexes (GII) are available on the World Health Organization's website (https://www.who.int/data/nutrition/nlis/info/gender-inequality-index-(gii)). For additional details, see Supplementary Data S1.

Research involving human participants, their data, or biological material

Policy information about studies with human participants or human data. See also policy information about sex, gender (identity/presentation), and sexual orientation and race, ethnicity and racism.

Reporting on sex and gender	Sex information was determined by self-report. No information regarding gender was inquired. We analyzed and reported sex differences between groups in brain age gaps. The total sample included 2970 female and 2336 male. Table 1 showed number of female and male in each subsample
Reporting on race, ethnicity, or other socially relevant groupings	No information regarding race or ethnicity was inquired. We did not considered race or ethnicity as a proxy of socioeconomic status.
Population characteristics	In this study, age, sex, and years of education covariates were considered for the human research participants. The full dataset included a total of 5306 participants, with 3509 healthy controls (HCs), 517 individuals with mild cognitive impairment (MCI), 828 individuals with Alzheimer's disease (AD), and 463 individuals with behavioral variant frontotemporal dementia (bvFTD). For the fMRI dataset, the age of participants varied significantly across groups. Non-LAC healthy controls had an average age of 53.55 years (SD = 13.43), while LAC healthy controls had an average age of 65.34 years (SD = 11.44). Non-LAC individuals with MCI had an average age of 59.62 years (SD = 8.77), compared to 66.53 years (SD = 8.18) for their LAC counterparts. Non-LAC individuals with AD had an average age of 76.59 years (SD = 9.35), whereas LAC individuals with AD had an average age of 77.52 years (SD = 9.35). Non-LAC individuals with bvFTD had an average age of 73.14 years (SD = 8.56), while LAC individuals with bvFTD had an average age of 73.15 years (SD = 8.76). Sex distribution also showed variability. Among non-LAC healthy controls, there were 470 females and 497 males, while LAC healthy controls included 261 females and 216 males. Non-LAC individuals with MCI had 114 females and 101 males, whereas LAC individuals with MCI had 84 females and 85 males. In the AD group, non-LAC individuals consisted of 112 females and 102 males, while LAC individuals included 262 females and 243 males. For bvFTD, non-LAC participants included 98 females and 92 males, and LAC participants included 105 females and 111 males. Years of education also varied among participants. Non-LAC healthy controls had an average of 13.15 years of education (SD = 5.41), while LAC healthy controls had an average of 12.11 years (SD = 3.39). Non-LAC individuals with MCI had an average of 14.15 years (SD = 3.41), compared to 11.52 years (SD = 6.32) for LAC individuals with MCI. Non-LAC individuals with AD had an average of 13.12 years (SD = 5.34), whereas LAC individuals with AD had an average of 8.89 years (SD = 4.34). Non-LAC individuals with bvFTD had an average of 11.16 years (SD = 3.56), while LAC individuals with bvFTD had an average of 7.89 years (SD = 3.36). For the EEG dataset, non-LAC healthy controls had an average age of 58.98 years (SD = 12.03), while LAC healthy controls had an average age of 66.74 years (SD = 13.94). Sex distribution in the EEG dataset showed that non-LAC healthy controls consisted of 470 females and 99 males. In the LAC healthy controls, there were 954 females and 532 males, with 111 females and 22 males among LAC individuals with MCI, 85 females and 23 males among LAC individuals with AD, and 39 females and 18 males among LAC individuals with bvFTD. Years of education for the EEG dataset also showed differences. Non-LAC healthy controls had an average of 14.85 years (SD = 4.91). LAC healthy controls had an average of 13.92 years (SD = 3.39), individuals with MCI had an average of 8.12 years (SD = 4.34), individuals with AD had an average of 10.75 years (SD = 6.32), and individuals with bvFTD had an average of 14.38 years (SD = 5.49).
Recruitment	Participants were selected following a stratified design in each country
Ethics oversight	The respective IRB of each institution that contributed EEGs and/or fMRIs to this study approved the acquisitions and protocols, and all the participants signed a consent form following the declaration of Helsinki.

Note that full information on the approval of the study protocol must also be provided in the manuscript.

Field-specific reporting

Please select the one below that is the best fit for your research. If you are not sure, read the appropriate sections before making your selection.

☒ Life sciences ☐ Behavioural & social sciences ☐ Ecological, evolutionary & environmental sciences

For a reference copy of the document with all sections, see nature.com/documents/nr-reporting-summary-flat.pdf

Life sciences study design

All studies must disclose on these points even when the disclosure is negative.

Sample size	The sample sizes for this study were determined using a data-driven approach to ensure the effectiveness of deep learning regressors in predicting brain age gaps. Preliminary analyses informed by pilot data and previous studies guided the decision to include a total of 5306 participants. This large sample size, encompassing 3509 healthy controls, 517 individuals with mild cognitive impairment, 828 individuals with Alzheimer's disease, and 463 individuals with behavioral variant frontotemporal dementia, provides a comprehensive dataset. This dataset captures the necessary variability for reliable model training and validation, enhancing the generalizability and predictive performance of the deep learning models. By leveraging such a sizable and diverse cohort, the study aims to develop models that can accurately predict brain age gaps across different populations and conditions, thereby ensuring robust and reliable outcomes.
Data exclusions	No data was excluded
Replication	The models were tested in six independent out of sample datasets. All attempts at replication were successful.
Randomization	Subsamples matched by age, sex, and education to the healthy control group.
Blinding	The investigators were blinded to group allocation during data collection and analysis.

Reporting for specific materials, systems and methods

We require information from authors about some types of materials, experimental systems and methods used in many studies. Here, indicate whether each material, system or method listed is relevant to your study. If you are not sure if a list item applies to your research, read the appropriate section before selecting a response.

Materials & experimental systems

n/a	Involved in the study
☒	☐ Antibodies
☒	☐ Eukaryotic cell lines
☒	☐ Palaeontology and archaeology
☒	☐ Animals and other organisms
☒	☐ Clinical data
☒	☐ Dual use research of concern
☒	☐ Plants

Methods

n/a	Involved in the study
☒	☐ ChIP-seq
☒	☐ Flow cytometry
☒	☐ MRI-based neuroimaging

Plants

Seed stocks	*Report on the source of all seed stocks or other plant material used. If applicable, state the seed stock centre and catalogue number. If plant specimens were collected from the field, describe the collection location, date and sampling procedures.*
Novel plant genotypes	*Describe the methods by which all novel plant genotypes were produced. This includes those generated by transgenic approaches, gene editing, chemical/radiation-based mutagenesis and hybridization. For transgenic lines, describe the transformation method, the number of independent lines analyzed and the generation upon which experiments were performed. For gene-edited lines, describe the editor used, the endogenous sequence targeted for editing, the targeting guide RNA sequence (if applicable) and how the editor was applied.*
Authentication	*Describe any authentication procedures for each seed stock used or novel genotype generated. Describe any experiments used to assess the effect of a mutation and, where applicable, how potential secondary effects (e.g. second site T-DNA insertions, mosiacism, off-target gene editing) were examined.*